ICAM

Institute for Computational and Applied Mechanics

STUDY OF MULTI-DIMENSIONAL RADIATIVE ENERGY TRANSFER IN MOLECULAR GASES

By

Jiwen Liu and S. N. Tiwari

NASA Grant NAG-1-363
NASA Langley Research Center
Hampton, Virginia 23681-0001

ODU/ICAM Report 93-102
October 1993

Old Dominion University
Norfolk, Virginia 23529-0247

PREFACE

This research was conducted in cooperation with the Fluid Mechanics Division of the NASA Langley Research Center during the period January 1992 to May 1993. The findings of this study were reported at the National Heat Conference in Atlanta, Georgia, August 1993.

The authors are indebted to Dr. John V. Shebalin of the Fluid Mechanics Division for his cooperation and technical assistance. Partial funding for this research was provided by the NASA Langley Research Center through the ICAM Program in Aeronautics, Grant NAG-1-363. The grant was monitored by Mr. Robert L. Yang, Assistant University Affairs Officer, Mail Stop 400, NASA Langley Research Center, Hampton, Virginia 23681-0001.

STUDY OF MULTI-DIMENSIONAL RADIATIVE ENERGY TRANSFER IN MOLECULAR GASES

By

Jiwen Liu[1] and S. N. Tiwari[2]

Department of Mechanical Engineering

Old Dominion University

Norfolk, VA 23529-0247

ABSTRACT

The Monte Carlo method(MCM) is applied to analyze radiative heat transfer in nongray gases. The nongray model employed is based on the statistical narrow band model with an exponential-tailed inverse intensity distribution. Consideration of spectral correlation results in some distinguishing features of the Monte Carlo formulations. Validation of the Monte Carlo formulations has been conducted by comparing results of this method with other solutions. Extension of a one-dimensional problem to a multi-dimensional problem requires some special treatments in the Monte Carlo analysis. Use of different assumptions results in different sets of Monte Carlo formulations. The nongray narrow band formulations provide the most accurate results.

1 Graduate Research Assistant.

2 Eminent Professor.

TABLE OF CONTENTS

NOMENCLATURE

Latin Symbols

b	length of a volume element, m
c	height of a volume element, m
H	height of parallel plates, m
I_ω	spectral radiative intensity, $kW/(m^2.sr.cm^{-1})$
k	line intensity to spacing ratio, $cm^{-1}.\ atm^{-1}$
L	slab thickness, m
L_{MB}	mean beam length, m
m	division numbers
M	number of elements for 1-D problem
MX, MY	number of elements in x, y directions
P	gas pressure, atm
$-dq_R/dy$	radiative dissipation for 1-D problem, kW/m^3
$-\nabla.q_r$	radiative dissipation, kW/m^3
q_w	net radiative wall flux, kW/m^2
Q	emitted radiative energy per unit volume, kW/m^3
R	random number
s, s′,s″	position variables, m
T	absolute temperature, K
U	pressure path length parameter, atm.m
x	mole fraction
y	y-coordinate, m

Greek symbols

β	line width to spacing ratio
γ	half-width of an absorption line, cm^{-1}
δ	equivalent line spacing, cm^{-1}
θ	polar angle
κ_ω	spectral absorption coefficient
μ	y-direction cosine=$\cos\theta$

ρ	reflectivity
τ_ω	spectral transmittance
ψ	azimuthal angle
ω	wavenumber, cm^{-1}
Ω	solid angle

LIST OF TABLES AND FIGURES

1. INTRODUCTION

There have been extensive research underway to develop hydrogen-fueled supersonic combustion ramjet (scramjet) propulsion systems for National Aero-Space Plane (NASP) at the NASA Langley Research Center. A critical element in the design of scramjets is the detailed understanding of the complex flowfield present in the different regions of the engine over a range of operating conditions. Numerical modeling of the flow in various sections has proven to be a valuable tool for gaining insight into the nature of these flows(Kumar, 1986; Drummond, 1986).

In a hypersonic propulsion system, combustion takes place at supersonic speeds to reduce the deceleration energy loss. The products of hydrogen-air combustion are gases such as water vapor and hydroxyl radical. These species are highly radiatively absorbing and emitting. Thus, numerical simulation must correctly handle the radiation phenomena associated with supersonic flows.

Radiative heat transfer is modeled by a radiative transfer equation with an absorption model. In the past three decades, a tremendous progress has been made in the field of radiative energy transfer in gray as well as nongray gaseous systems. As a results, several useful books (Sparrow and Cess, 1978; Siegel and Howell, 1981) and review articles (Edwards, 1983; Chan, 1987; Howell, 1988) have become available for engineering applications. In the sixties and early seventies, radiative transfer analyses were limited to one-dimensional cases. Including only one-dimensional radiation is very questionable for the most practical applications. Since the mid seventies, efforts have been directed towards formulating efficient and accurate multi-dimensional equations for radiative transfer. Great achievements have been made for gray gaseous systems. However, the studies on multi-dimensional nongray gaseous systems encounter tremendous difficulties and little progress has been made so far. A survey of various methods for mutil-dimensional radiative transfer analysis has been made by Howell (1983, 1988). Discussion were made regarding the feasibility of incorporating the spectral integration in the techniques using narrow band (Goody, 1964) and wide band models (Chan and Tien, 1969; Edwards and

Morizumi, 1970). Another review (Chan, 1987) has provided details of several methods that could possibly be applied to multi-dimensional radiative transfer in molecular participating media. Different review articles have unanimously indicated that one of the most promising methods to investigate the nongray participating media in multi-dimensional systems is the Monte Carlo method (MCM).

The MCM is a probabilistic method which can exactly simulate all important physical processes. In this method, the numerical treatment of mathematical formulation is easy and the usual difficulties encountered in complex geometries can be circumvented easily. It is due to these advantages that the MCM has been applied to solve many radiative transfer problems. The earliest application of this method for radiative transfer problems was made by Howell and Perlmutter (1964a). Radiative problems of increasing complexity which have been investigated by this method have appeared in the literature (Perlmutter and Howell, 1964; Howell and Perlmutter, 1964b; Steward and Cannon, 1971; Dunn, 1983; Gupta et al., 1983). Studies on reducing the computational time by using this method are also available (Kobiyama et al., 1979; Kobiyama et al., 1986). The gray gas assumption, however, is made in most of these analyses.

Like any other numerical methods, the MCM also has some disadvantages. One of them is the large appetite for computer time, and another is the statistical fluctuation of the results. With the rapid development of computers, these two disadvantages are becoming of less concerns and the interests in the MCM are becoming stronger. One of the recent applications of the MCM has been in the investigation of radiative interactions in nongray participating mediums using a narrow band model. For example, Taniguchi et al. (1991) applied a simplified from of the Elsasser narrow band model to investigate the problem of radiative equilibrium in a parallel plates system. Farmer and Howell (1992) obtained a Monte Carlo solution of radiative heat transfer in a three-dimensional enclosure with an anisotropically scattering, spectrally dependent, inhomogeneous medium. Modest (1992) discussed the effects of the narrow band averaging on the surface and medium emissions. It was pointed out that the narrow band model may be applied successfully to the MCM after verification in an isothermal and homogeneous medium.

However, all these studies have failed to reflect some fundamental mechanisms of the MCM in conjunction with a narrow band model, and the application of the MCM on nongray radiation problems is still uncertain.

The objective of this study is to employ a general and accurate narrow band model to investigate radiative heat transfer using the MCM. The same nongray model has been applied to investigate radiation contributions using the discrete direction method (Zhang et al., 1988) and S-N discrete ordinates method (Kim et al., 1991a). The present investigation includes derivation of the Monte Carlo statistical relationships, discussion of the fundamental features that are different from other methods and demonstration of the capability of the MCM for nongray analysis. One-dimensional problem is considered in the study first, and then the formulations are extended to a specific multi-dimensional problem. The analytical procedure developed in this study can be applied to systems with any irregular geometry. In the future work, the present analysis will be extended to the problems of combined transfer processes in chemically reacting flows such as those in scramjet propulsion systems.

For the present study, the information on radiation absorption models is given in Sec. 2. Analysis of the MCM with a narrow band model is provided in Sec. 3. Validation of this analysis is presented in Sec. 4. The extension of MCM formulations to a specific two-dimensional problem is provided in Sec. 5.

2. RADIATION ABSORPTION MODEL

The study of radiative transmission in nonisothermal and inhomogeneous gaseous systems requires a detailed knowledge of the absorption, emission and scattering characteristics of the specific gas. Several models are available in the literature to represent the absorption emission characteristics of molecular species. The gray gas model is the simplest model to employ in radiative transfer analyses. In this model, the absorption coefficient is assumed to be independent of wavenumber. In many practical applications, the radiative transfer by hot molecular gases such as H_2O and CO_2 involves vibration-rotation bands that are difficult to model by a gray gas model due to the strong wavenumber dependent properties of the bands.

The nongray gas models account for the effect of wavenumber on absorption coefficient. Based on the range of the wavenumber interval within which the absorption coefficient is calculated, the nongray models can be line-by-line models, narrow band models, and wide band models. The line-by-line models are theoretically the most precise models to treat radiative heat transfer. But solutions of the line-by-line formulation require considerably large computational resources. Consequently, it is not practical to apply the line-by-line models in most engineering problems.

The narrow band models can quite accurately represent the absorption within a narrow band interval of a vibration rotation band and they are much simper than the line-by-line models. Four usually employed narrow band models are Elsasser, statistical, random-Elsasser and qusi-random narrow band models. Various wide and narrow band models have been tested with the results of line-by-line calculations in the literature (Tiwari, 1978; Soufiani et al., 1985; Soufiani and Taine, 1987). Accurate results for temperature and heat flux distribution are obtained with the statistical narrow band model which assumes the absorption lines to be randomly placed and the intensities to obey an exponential-tailed-inverse distribution. The transmittance of a homogeneous and isothermal column of length l due to gas species j, averaged over $[\omega—(\Delta\omega/2)$,

$\omega+(\Delta\omega/2)]$, is then given by (Malkmus, 1967)

$$\bar{\tau}_{\omega}^{j} = exp\left[-\frac{\bar{\beta}}{\pi}\left(\sqrt{\left(1+\frac{2\pi x_j P l \bar{k}}{\bar{\beta}}\right)}-1\right)\right] \tag{2.1}$$

where x_j represents the mole fraction of the absorbing species j and P is total pressure; $\bar{k}$ and $\bar{\beta} = 2\pi\bar{\gamma}/\bar{\delta}$ are the band model parameters which account for the spectral structure of the gas. The overbar symbol indicates that the quantity is averaged over a finite wavenumber interval $\Delta\omega$. Parameters $\bar{k}$ and $1/\bar{\delta}$ generated from a line-by-line calculation have been published for H_2O and CO_2 (Ludwig et al., 1973; Hartmann et al., 1984; Soufiani et al., 1985). The mean half-width $\bar{\gamma}$ is obtained using the parameters suggested by Soufiani et al. (1985). The narrow band width considered is usually 25 cm^{-1}.

The wide band models are the simplest nongray models and are extensively used in radiative heat transfer analyses (Cess et al., 1967; Buckius, 1982). Four commonly used wide band models are box, modified box, exponential and axial wide band models. By far the most popular wide band model is the exponential wide band model developed by Edwards (1976). Edwards and co–workers (Edwards and Menard, 1964; Edwards and Babikian, 1989), as well as other investigators (Thynell, 1989), have successfully used this model. The exponential wide band model accounts for discrete absorption bands and spectral correlations resulting from the high resolution structure. However, the spectral discretization used in this model is too wide and it does not take into account the low resolution correlations between intensities and transmissivities (Soufiani and Taine, 1987). Also, the case of partially reflecting walls cannot be correctly modelled with this approach (Edwards, 1976). These two disadvantages are avoided when a statistical narrow band model is used in radiative transfer calculations (Soufiani and Taine, 1987). Therefore, the narrow band model formulation expressed by Eq. (2.1) is employed in this study to investigate nongray radiation problems.

For a nonisothermal and inhomogeneous column, the Curtis-Godson approximation (Godson, 1953) leads to accurate results if pressure gradients are not too large. Basically, this approach consists of transformation of such a column into an equivalent isothermal and homogeneous one.

For the narrow band model expressed in Eq. (2.1), effective band model parameters $\bar{k}_e$ and $\bar{\beta}_e$ are introduced by averaging $\bar{k}$ and $\bar{\beta}$ over the optical path U of the column as

$$U(l) = \int_0^l P(y)x_j(y)dy \tag{2.2}$$

$$\bar{k}_e = \frac{1}{U(l)} \int_0^l P(y)x_j(y)\bar{k}(y)dy \tag{2.3}$$

$$\bar{\beta}_e = \frac{1}{\bar{k}_e U(l)} \int_0^l P(y)x_j(y)\bar{k}(y)\bar{\beta}(y)dy \tag{2.4}$$

The transmittance of this equivalent column is then calculated from Eq. (2.1).

3. MONTE CARLO SIMULATION USING A NARROW BAND MODEL

To investigate radiative heat transfer using the MCM and a narrow band model, a simple problem is considered at first. Figure 3.1 shows an absorbing and emitting molecular gas between two infinite parallel plates with the slab thickness of L. Temperature, concentration and pressure in the medium are supposed to be known. The walls are assumed to be diffuse but not necessarily gray. The wall temperature is also known. Usually, the radiative transfer quantities of interest are the net radiative wall flux and the radiative dissipation inside the medium. The radiative dissipation is nothing but the divergence of radiative heat flux with opposite sign. In order to calculate these quantities, the medium considered is divided into (M−2) volume elements. The grid numbers on the lower and upper walls are 1 and M, respectively. Temperature, concentration and pressure are assumed to be constant in each volume element. The typical method for handling radiative exchange between surface and/or volume elements is to evaluate the multiple integral which describes the exchange by some type of numerical integration technique. This, usually, is a good approach for simple problems. An alternate method is used here. Radiative transfer in the computational domain is simulated using the MCM.

The MCM uses a large number of bundles of energy to simulate the actual physical processes of radiant emission and absorption of energy occurring in a medium. These energy bundles are similar to photons in their behavior. The histories of these energy bundles are traced from their point of emission to their point of absorption. What happens to each of these bundles depends on the emissive, scattering and absorptive behavior within the medium which is described by a set of statistical relationships. The net radiative wall flux or the radiative dissipation in an element is equal to the total radiative energy absorbed in this element minus its emitted radiative energy, divided by the area or the volume of the element.

The use of a narrow band model in the MCM presents new features in the analysis of radiative heat transfer. The statistical relationships currently in use need to be modified. The following Monte Carlo analyses are based on an arbitrarily chosen finite volume element. The

statistical relationships for an energy bundle emitted from a surface element can be derived by following the same procedure.

3.1. Monte Carlo Formulation

Let us consider the Planck spectral blackbody intensity $I_{b\omega}$ that enters the ith volume element at the point s on the lower side and intersects the upper side at the point s′ as shown in Fig. 3.1. A spherical coordinate system is established and centered at the point s. Under the condition of local thermodynamic equilibrium, an amount of energy absorbed in a finite volume element is equal to that emitted. Thus, the amount of energy emitted for a wavenumber range $d\omega$ and along a pencil of column s→s′ with a solid angle increment $d\Omega$ is expressed as

$$dQ_i = I_{b\omega}\left[1 - \tau_\omega(s \rightarrow s')\right] \cos\theta d\Omega d\omega \tag{3.1}$$

where τ_ω(s→s′) is the spectral transmittance over the path s→s′, θ is the polar angle between the y axis and the direction of the column s→s′, and $d\Omega = \sin\theta d\theta d\psi$ where ψ is the azimuthal angle. The total emitted energy per unit volume is obtained by integrating Eq. (3.1) over the wavenumber, polar, and azimuthal angle as (Howell, 1968; Siegel and Howell, 1981; Haji-Sheikh, 1988)

$$\begin{aligned} Q_i &= \int_0^\infty \int_0^\pi \int_0^{2\pi} I_{b\omega}\left[1 - \tau_\omega(s \rightarrow s')\right] \cos\theta \sin\theta d\psi d\theta d\omega \\ &= 2\pi \int_0^\infty \int_0^\pi I_{b\omega}\left[1 - \tau_\omega(s \rightarrow s')\right] \cos\theta \sin\theta d\theta d\omega \\ &= 2\pi \int_0^\infty \int_{-1}^1 I_{b\omega}[1 - \tau_\omega(\Delta y_i/\mu)]\mu d\mu d\omega; \quad \mu = \cos\theta \end{aligned} \tag{3.2}$$

where Δy_i is the thickness of ith volume element. It should be noted that the sign of Δy_i is different when μ varies from positive to negative.

The simulation of an energy bundle includes the determination of wavenumber and direction of emission of this energy bundle in the finite volume element. The statistical relationships for

determining these parameters are readily obtained from Eq. (3.2) as

$$R_\omega = \frac{2\pi \int_0^\omega \int_{-1}^{1} I_{b\omega}[1 - \tau_\omega(\Delta y_i/\mu)]\mu d\mu d\omega}{Q_i} \tag{3.3}$$

$$R_\mu = \frac{2\pi \int_\mu^1 \int_0^\infty I_{b\omega}[1 - \tau_w(\Delta y_i/\mu)]\mu d\omega d\mu}{Q_i} \tag{3.4}$$

where R_ω and R_μ are random numbers which are uniformly distributed between zero and one. In Eqs. (3.2)-(3.4), τ_ω is a real spectral transmittance. Before solving these equations to obtain ω and μ from a set of given values of R_ω and R_μ, the narrow band model should be applied to approximate the real spectral transmittance.

For the narrow band model, the absorption bands of the gas are divided into spectral ranges $\Delta\omega$ wide; each is centered at ω^k and characterized by the superscript k; the band parameters obtained are the averaged quantities over a narrow band. So, the spectral quantities in Eqs. (3.2)-(3.4) should be transformed into the averaged quantities over a narrow band for practical applications. Taking the spectral average over all narrow bands, Eqs. (3.2)-(3.4) are expressed as

$$Q_i = 2\pi \sum_{k=1}^{m_\omega} \left\{ \int_{-1}^{1} \overline{I_{b\omega^k}}[1 - \overline{\tau_{w^k}}(\Delta y_i/\mu)]\mu d\mu \right\} \Delta\omega^k \tag{3.5}$$

$$R_\omega = \frac{2\pi \sum_{k=1}^{n} \left\{ \int_{-1}^{1} \overline{I_{b\omega^k}}[1 - \overline{\tau_{\omega^k}}(\Delta y_i/\mu)]\mu d\mu \right\} \Delta\omega^k}{Q_i}, \quad (\omega^{n-1} < \omega \leq \omega^n) \tag{3.6}$$

$$R_\mu = \frac{2\pi \sum_{k=1}^{m_\omega} \left\{ \int_{\mu}^{1} \overline{I_{b\omega^k}}[1 - \overline{\tau_{w^k}}(\Delta y_i/\mu)]\mu d\mu \right\} \Delta\omega^k}{Q_i} \tag{3.7}$$

where m_ω is the total number of narrow bands. The following narrow band approximation has been used in obtaining Eqs. (3.5)-(3.7)

$$\overline{I_{b\omega^k}\tau_{w^k}} = \frac{1}{\Delta\omega^k} \int_{\Delta\omega^k} I_{b\omega}\tau_\omega d\omega$$

$$\approx \overline{I_{b\omega^k}}\left(\frac{1}{\Delta\omega^k}\int_{\Delta\omega^k}\tau_\omega d\omega\right)$$
$$= \overline{I_{b\omega^k}}\,\overline{\tau_{w^k}} \tag{3.8}$$

This is because $I_{b\omega}$ is essentially constant over a narrow band and may be taken out of the spectral integral. Otherwise, the average product $\overline{I_{b\omega^k}\tau_{\omega^k}}$ is not equal to the product of $\overline{I_{b\omega^k}}$ and $\overline{\tau_{\omega^k}}$.

Equations (3.6) and (3.7) are solved for ω and μ each time a set of values of R_ω and R_μ are chosen. The computing time becomes too large for practical calculations since the integrands in these equations are very complex functions of integration variables and the number of energy bundles usually is very large. To circumvent this problem, interpolation and approximation methods are employed. For example, to obtain the value of ω for a given value of R_ω, we first choose different values of ω and obtain the corresponding values of R_ω from Eq. (3.6). Then, a smooth curve is constructed to match these data points, and ω values are easily obtained from this curve for selected values of R_ω. The procedures for determining μ are similar to those for ω.

Following the determination of wavenumber and direction of an energy bundle, it is essential to find the location of absorption of the energy bundle in the participating medium. Let us still consider the emitted radiant energy along a pencil of column s→s′ (Fig. 3.1). After this amount of energy is transmitted over a column s′→s″, the remaining radiant energy is given by

$$dQ'_i = I_{b\omega}\left[1-\tau_\omega(s\to s')\right]\tau_\omega(s'\to s'')\cos\theta d\Omega d\omega \tag{3.9}$$

where τ_ω(s′→s″) is the spectral transmittance over the path s′→s″. Taking a narrow band average over Eqs. (3.1) and (3.9) and dividing the latter one with the first one, the statistical relationship for determining the location of absorption can be expressed as

$$R_l = \frac{\overline{[1-\tau_\omega(s\to s')]\tau_\omega(s'\to s'')}}{1-\overline{\tau_\omega}(s\to s')}$$
$$= \frac{\overline{\tau_\omega}(s'\to s'') - \overline{\tau_\omega(s\to s')\tau_\omega(s'\to s'')}}{1-\overline{\tau_\omega}(s\to s')} \tag{3.10}$$

where R_l is a random number. The averaged product $\overline{\tau_\omega(s\to s')\tau_\omega(s'\to s'')}$ is not equal to the product of $\overline{\tau_\omega(s\to s')}$ and $\overline{\tau_\omega(s'\to s'')}$ because the $\tau_\omega(s\to s')$ and $\tau_\omega(s'\to s'')$ have a

strong wavenumber dependence due to the high resolution structure in a very small range of an absorption band (hundreds of major absorption lines in a 25 cm^{-1} spectral interval), and must be treated in a spectrally correlated way. Equation (3.10) can be simplified as

$$R_l = \frac{\overline{\tau_\omega}(s' \rightarrow s'') - \overline{\tau_\omega}(s \rightarrow s'')}{1 - \overline{\tau_\omega}(s \rightarrow s')} \tag{3.11}$$

If the spectral correlation between $\tau_\omega(s \rightarrow s')$ and $\tau_\omega(s' \rightarrow s'')$ is not taken into account, then Eq. (3.10) becomes

$$R_l = \overline{\tau_\omega}(s' \rightarrow s'') \tag{3.12}$$

Equation (3.12) is the statistical relationship usually employed for determining the location of absorption in the Monte Carlo simulation and is quite different from Eq. (3.11). For an isothermal and homogeneous medium, the travelling distance of an energy bundle can be obtained directly by solving Eq. (3.11) for a given random number. But this procedure turns out to be somewhat complicated for a nonisothermal and inhomogeneous medium. It becomes necessary to try each volume element starting from the adjacent element of the location where an energy bundle emits until a finite volume element is found in which Eq. (3.11) can be satisfied.

3.2. Special Features of MCM for Nongray Analysis

The MCM is quite different from other numerical techniques for the analysis of radiative heat transfer. Its characteristics have been discussed in detail by Siegel and Howell (1981). Use of a nongray model in the radiative transfer analysis requires significant changes. Two special features of incorporating the nongray model in the MCM are discussed here.

Most of the existing analyses in radiative heat transfer start with the transfer equation of the type given by Siegel and Howell (1981). In order to apply a narrow band model, this equation has to be spectrally averaged over a narrow band. This averaging treatment results in two kinds of spectral correlations. One is the spectral correlation between the intensity and the transmittance within the medium. Another is the spectral correlation between the reflected component of the wall radiosity and the transmittance. In order to investigate the first kind of

spectral correlation, all the intermediate transmittances in each finite volume element of medium along the path the radiative energy travels must be calculated and stored to make a correlated calculation. In order to investigate the second kind of spectral correlation, a series expansion of the wall radiosity is required. Essentially, this series expansion is utilized along with a technique for closure of the series.

The simulation of radiative heat transfer in the MCM is not directly based on the radiative transfer equation. This results in the MCM having features different from the other methods for nongray analysis. When the radiative energy is transmitted in the medium, the spectral correlation does occur in the MCM, but it occurs between the transmittances of two different segments of the same path which is different from other methods. This is the first feature with the MCM for nongray analysis.

The MCM procedures are based on the direct simulation of the path of an energy bundle. For the case with reflecting walls, the mechanism of the reflections simulation in the MCM is the same as a series expansion of the wall radiosity. However, this simulation process becomes much simpler because of a probabilistic treatment. Also, there are no spectrally correlated quantities involved. This is the second feature of the MCM for nongray analysis. Exact treatment of the reflections in the MCM in nongray gases is the same as that in gray gases and may be found in the literature (Howell, 1968; Siegel and Howell, 1981).

The second feature of the MCM allows one to obtain results for a reflecting wall with very little increase in the computation time compared to that for a nonreflecting wall. But in other methods, the consideration of the history of a finite number of reflections and approximating the remaining reflections by a closure method in the radiative transfer equation complicates the mathematical formulation and increases the computer time considerably. As the geometry considered becomes complicated, exact simulation of radiative heat transfer in the case with reflecting wall will be very difficult for most existing methods, while it is not a big problem for the MCM. So, it seems that the MCM is able to retain the feature of simplicity in dealing with the complicated problems while a narrow band model is employed.

4. VALIDATION OF MONTE CARLO ANALYSIS

In order to validate the Monte Carlo simulation along with a narrow band model, results for radiative dissipation inside the medium and the net radiative wall heat flux have been obtained for different temperature and concentration profiles with nonreflecting and reflecting walls. In this work, the reflectivities of two parallel diffuse walls are assumed to be identical and are denoted by the symbol ρ. Three different temperature profiles are used here and these are uniform, boundary layer type and parabolic profiles (Fig. 3.2). They are obtained from Kim et al. (1991a) and Menart et al. (1993). For the uniform temperature profile, the gas temperature is chosen to be 1000 K, while the walls are held at 0 K. Also shown in the figure is a parabolic H_2O concentration profile for a mixture of H_2O and N_2 at 1 atm, and it is also taken from the above cited references. A uniform composition of pure H_2O vapor at 1 atm is another H_2O concentration profile used. Several cases with the selected temperature and H_2O concentration profiles have been considered previously using the S-N discrete ordinates method by including all important bands. The Monte Carlo solutions are compared with the available solutions for identical conditions.

In the Monte Carlo simulation, the entire slab of the physical problem is divided into 20 sublayers for all calculations. Further subdivision of the computation domain yields little changes in the results. The computation were performed on a Sun Sparc workstation. The number of total energy bundles for each case was chosen to be 50,000. This choice represents a compromise between accuracy and saving of computation time. When the relative statistical errors of the results were chosen to be less than ±3%, the probability of the results lying within these limits was greater than 95%. The computing times for the correlated and noncorrelated formulations were essentially the same. For an isothermal and homogeneous medium, the required CPU time was about 1–2 minutes for each case. For nonisothermal and inhomogeneous medium, the CPU time was increased to 5–7 minutes, and it was nearly 10 minutes for the case with strongly reflecting walls (ρ=0.9) and large optical length (L=0.5 m).

The situation with nonreflecting walls is considered first. Figures 3.3(a)-3.3(c) show the comparisons between the Monte Carlo solutions and S-N discrete ordinates solutions. Four different S-N discrete ordinates solutions are available in the literature (Kim et al., 1991a) which employ different band models. For our comparison, we selected the solution — S-20 nongray narrow band solution because it employs the same narrow band model as used in this study.

Figure 3.3(a) and 3.3(b) show the radiative dissipation results obtained for the uniform temperature and uniform pure H_2O vapor distribution with the slab thickness of 0.1 m and 1.0 m, respectively. The Monte Carlo results essentially match the S-N discrete ordinates results. Figure 3.3(c) presents the results with the boundary layer type temperature profile and for the same concentration distribution as in Figs. 3.3(a) and 3.3(b). The Monte Carlo results predict the same change of gas behavior (from a net emitter near the hot wall to a net absorber away from the hot wall) as the S-N discrete ordinates results. The results for the parabolic H_2O concentration distribution (with a uniform temperature profile) are shown in Fig. 3.3(d). The Monte Carlo method also predicts the interesting W type shape distribution of $-\partial q_R/\partial y$ as in the S-N discrete ordinates method. Here the Monte Carlo solutions appear to be a little higher than the S-N discrete ordinates solutions, especially in the central region.

The results for the net radiative wall heat flux obtained for the cases presented in Figs. 3.3(a)-3.3(d) are given in Table 3.1. The differences of results between different solutions for the three cases are not more than 3.5%. This shows agreement similar to that for the radiative dissipation results.

The situation with reflecting walls is considered next. Figures 3.4(a)–3.4(e) show the comparisons between the Monte Carlo solutions and the S-N discrete ordinates solutions for different wall reflectivities and slab thicknesses. For these results, the parabolic type temperature profile and the uniform composition of pure H_2O vapor at 1 atm are assumed. The S-N discrete ordinates solutions are based on the second-degree closure results (Menart et al., 1993). The second-degree closure means that the history of two reflections is considered in the radiative flux equation and the remaining reflections are approximated by a closure method. Based on

the study by Kim et al. (1991b), the second-degree discrete ordinates solutions for typical cases required about 160 minutes on the Cray-2 supercomputer. This is significantly higher than the CPU time required for the MCM, which is not more than 10 minutes on a Sun Sparc workstation.

Table 3.1 Comparison of net radiative wall heat fluxes with nonreflecting walls (kW/m^2)

	Monte Carlo	S-N Discrete Ordinates
Uniform T; L=0.1 m	-14.2	-14.3
Unifrom T; L=1.0 m	-27.6	-28.2
Boundary layer T	280.4	277.4
Uniform T with concentration profile	-24.5	-25.4

Figures 3.4(a)–3.4(c) present the results of $-\partial q_R/\partial y$ for the wall reflectivities of ρ= 0.1, 0.5 and 0.9 respectively, , with the slab thickness of L=0.5m. Excellent agreements between different solutions are seen in the figures. In the central region, the values of $-\partial q_R/\partial y$ are approaching a plateau. The Monte Carlo results appear to be slightly oscillating in this region. The reason is that the total number of energy bundles is a finite number and the Monte Carlo results are of statistical nature. The oscillation decreases and the results of $-\partial q_R/\partial y$ become smoother as the total number of energy bundles is increased. This oscillation is also found in other figures. Figure 3.4(d) and 3.4(e) show the results for the same strongly reflecting walls of ρ=0.9 with the slab thicknesses of L=0.1 m and L=1.0 m, respectively. Again, the Monte Carlo solutions appear very close to the S-N discrete ordinates solutions.

Table 3.2 shows the net radiative wall heat fluxes for the cases presented in Figs. 3.4(a)-3.4(e). The Monte Carlo results are slightly lower than the S-N discrete ordinates results. But the differences are within 6%. There are physical justifications for such discrepancies. In the S-N discrete ordinates method, the history of two reflections is taken into account and the

remaining reflections are approximated as travelling in a medium without any attenuation. This approximation overpredicts the radiative energy absorbed on the walls. In the MCM, the history of the reflections is simulated in an exact manner. In addition, the Monte Carlo solutions are also subject to small statistical errors.

Table 3.2 Comparison of net radiative wall heat fluxes with reflecting walls (kW/m^2)

	L (m)	Monte Carlo	S-N Discrete Ordinates
ρ=0.1	0.5	14.42	15.12
ρ=0.5	0.5	9.47	9.66
ρ=0.9	0.1	2.22	2.34
	0.5	2.55	2.70
	1.0	2.58	2.67

The spectrally correlated results are compared with the noncorrelated results in Figs. 3.5(a) and 3.5(b). A spectral correlation has been considered in all the results presented in previous figures. In a spectrally noncorrelated formulation, the correlation between spectrally dependent quantities is neglected. By using Eq. (3.12), the Monte Carlo noncorrelated results can be obtained. The temperature and H_2O concentration distributions considered here are the same as those in Figs. 3.4(a) and 3.4(b). The wall reflectivities are ρ=0.0 for Fig. 5(a) and ρ=0.5 for Fig. 3.5(b) , and the slab thickness L is 0.1 m for the two cases. The figures clearly show that the noncorrelated results overestimate the gas emission in the central region, and differ by about 30–35% from the correlated results. The reason for this discrepancies is in the derivation of the statistical relationship for determining the location of absorption of an energy bundle. The term $\overline{\tau_\omega(s \rightarrow s')\tau_\omega(s' \rightarrow s'')}$ in Eq. (3.10) can be treated in two different ways, that is, $\overline{\tau_\omega(s \rightarrow s')\tau_\omega(s' \rightarrow s'')} = \overline{\tau_\omega}(s \rightarrow s'')$ and $\overline{\tau_\omega(s \rightarrow s')} \cdot \overline{\tau_\omega(s' \rightarrow s'')}$, respectively. The first choice results in the correlated formulation given by Eq. (3.11) and the second choice results in the noncorrelated formulation given by Eq. (3.12). Since the value of $\overline{\tau_\omega(s \rightarrow s')\tau_\omega(s' \rightarrow s'')}$ is

greater than the value of $\overline{\tau_\omega(s \rightarrow s')} \cdot \overline{\tau_\omega(s' \rightarrow s'')}$, the R_l calculated from Eq. (3.11) is smaller than that calculated from Eq. (3.12) for the same conditions. This means that an energy bundle travels a shorter distance by using the correlated formulation in comparison to that by using the noncorrelated formulation. So, it is concluded that an energy bundle is more likely to be absorbed near the point of emission for the correlated case and near or on the walls for the noncorrelated case. Because correlated results and noncorrelated results differ significantly, the spectral correlation must be taken into account in order to predict the radiative heat transfer accurately.

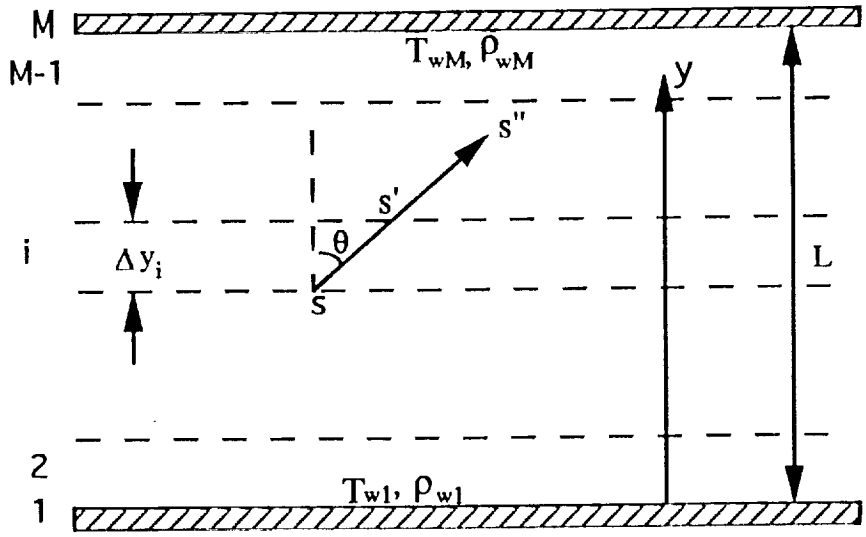

Fig. 3.1 Planar medium between two parallel walls

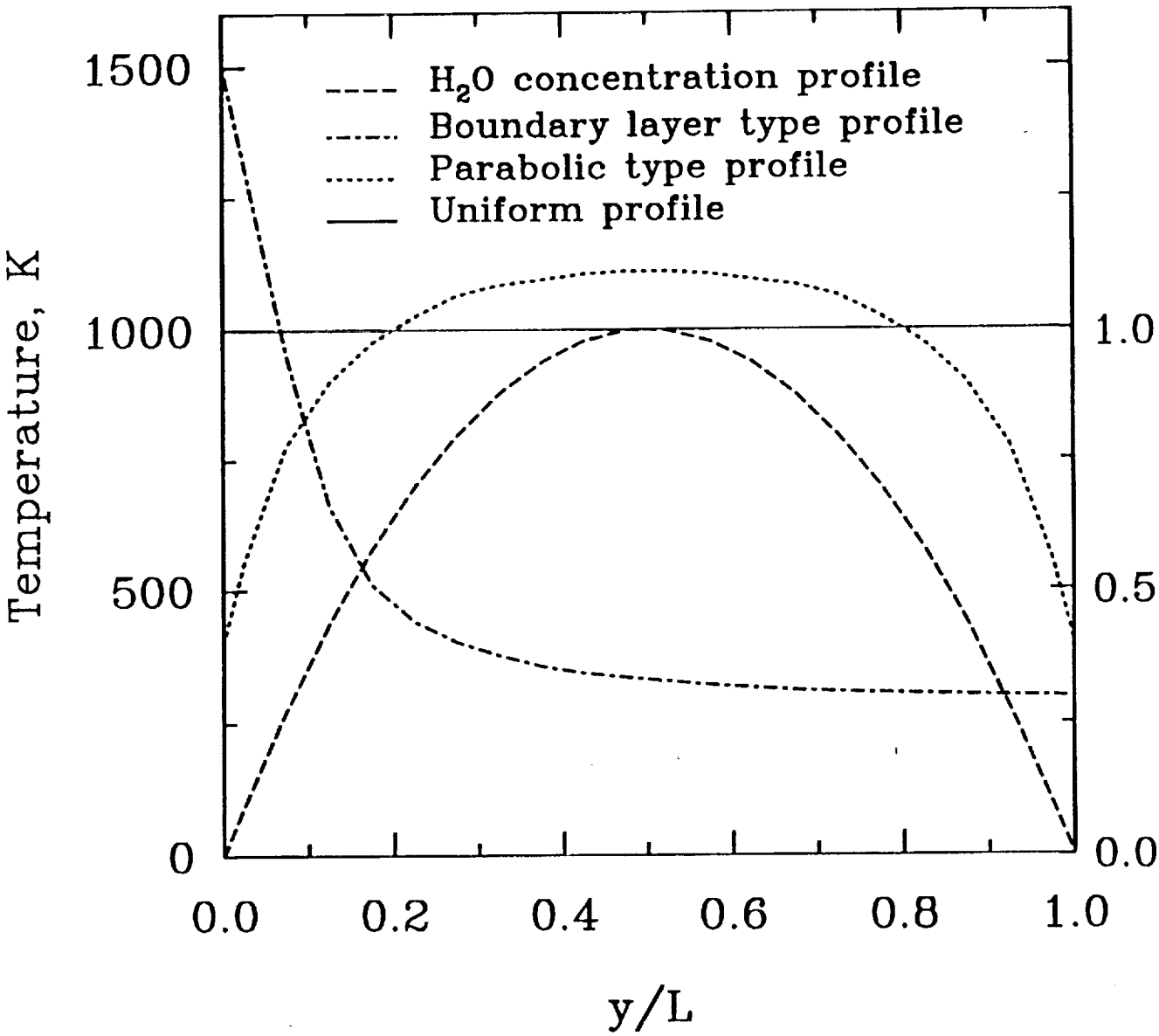

Fig.3.2 Temperature and concentration profiles.

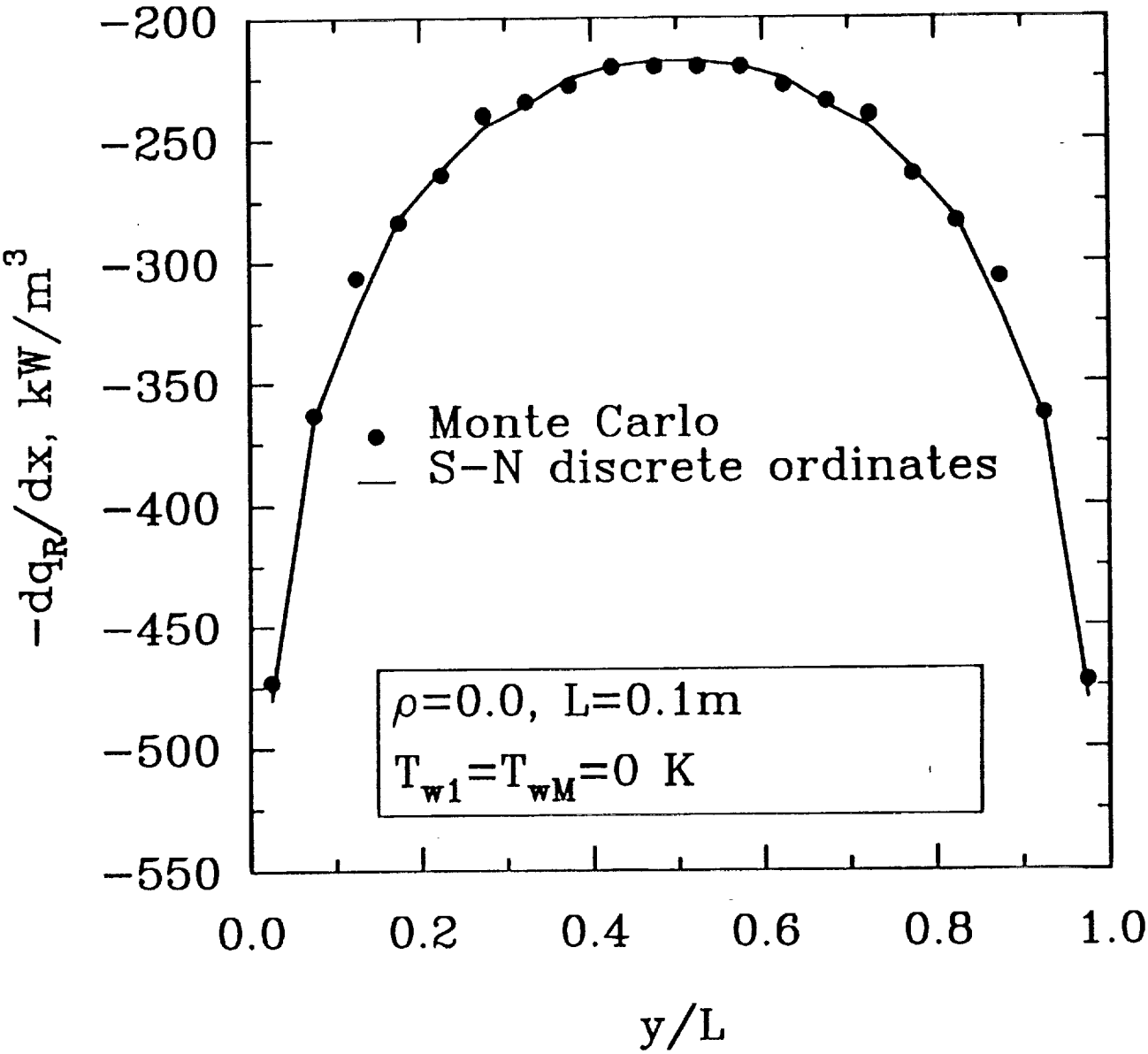

Fig. 3.3(a) Comparison of radiative dissipation for the uniform temperature profile with L=0.1m.

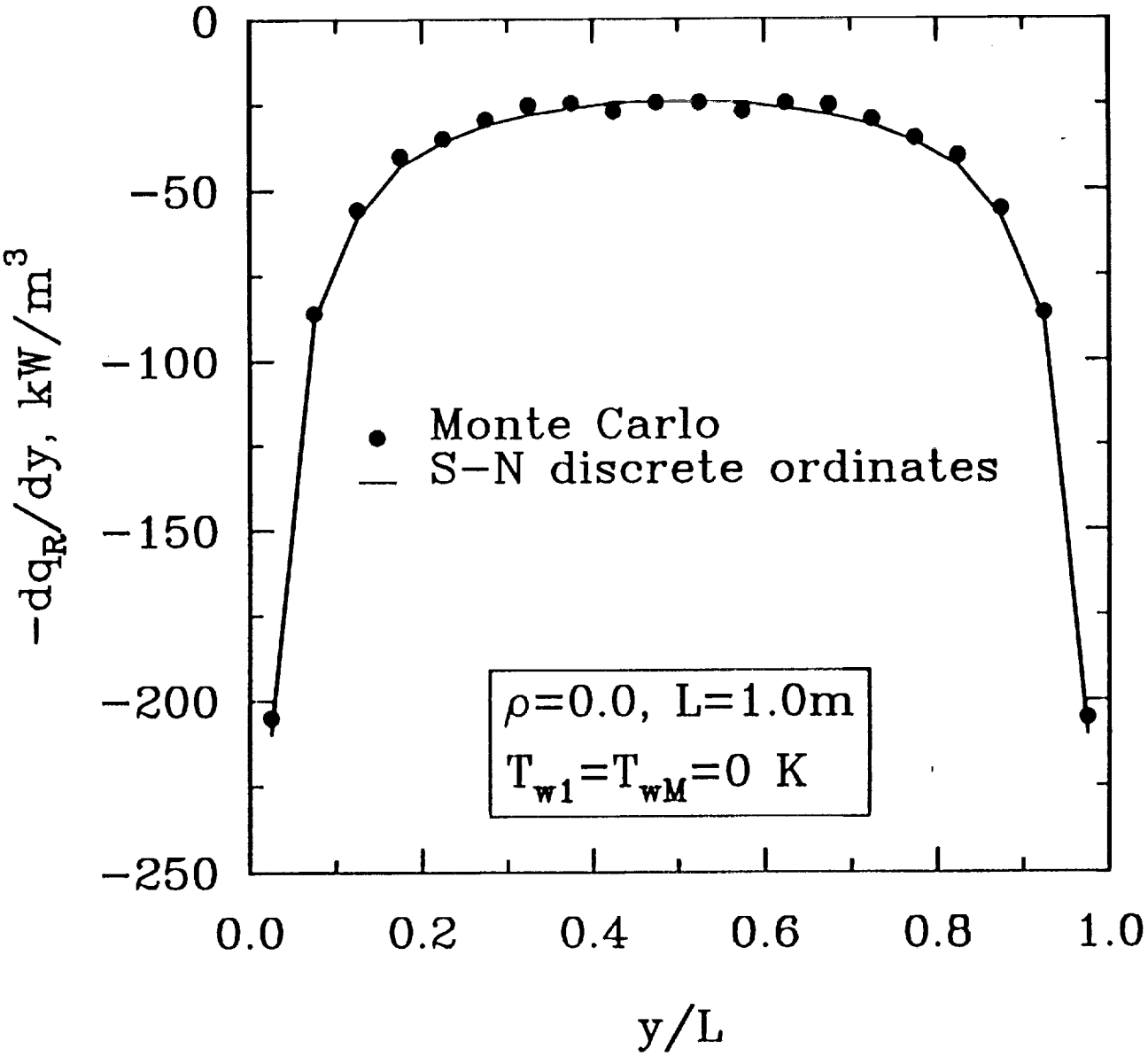

Fig. 3.3(b) Comparison of radiative dissipation for the uniform temperature profile with L=1.0 m.

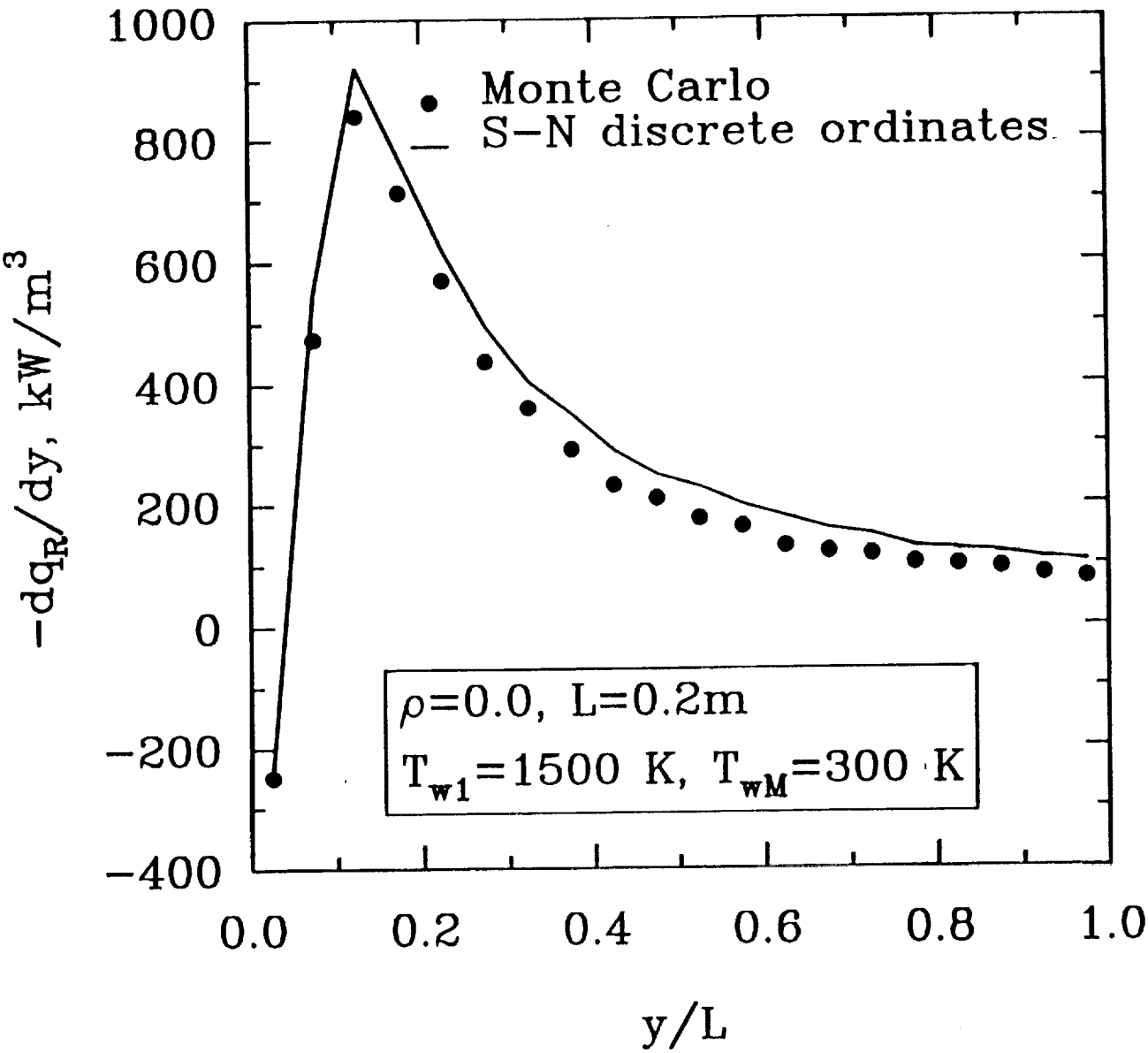

Fig. 3.3(c) Comparison of radiative dissipation for the boundary layer type temperature profile.

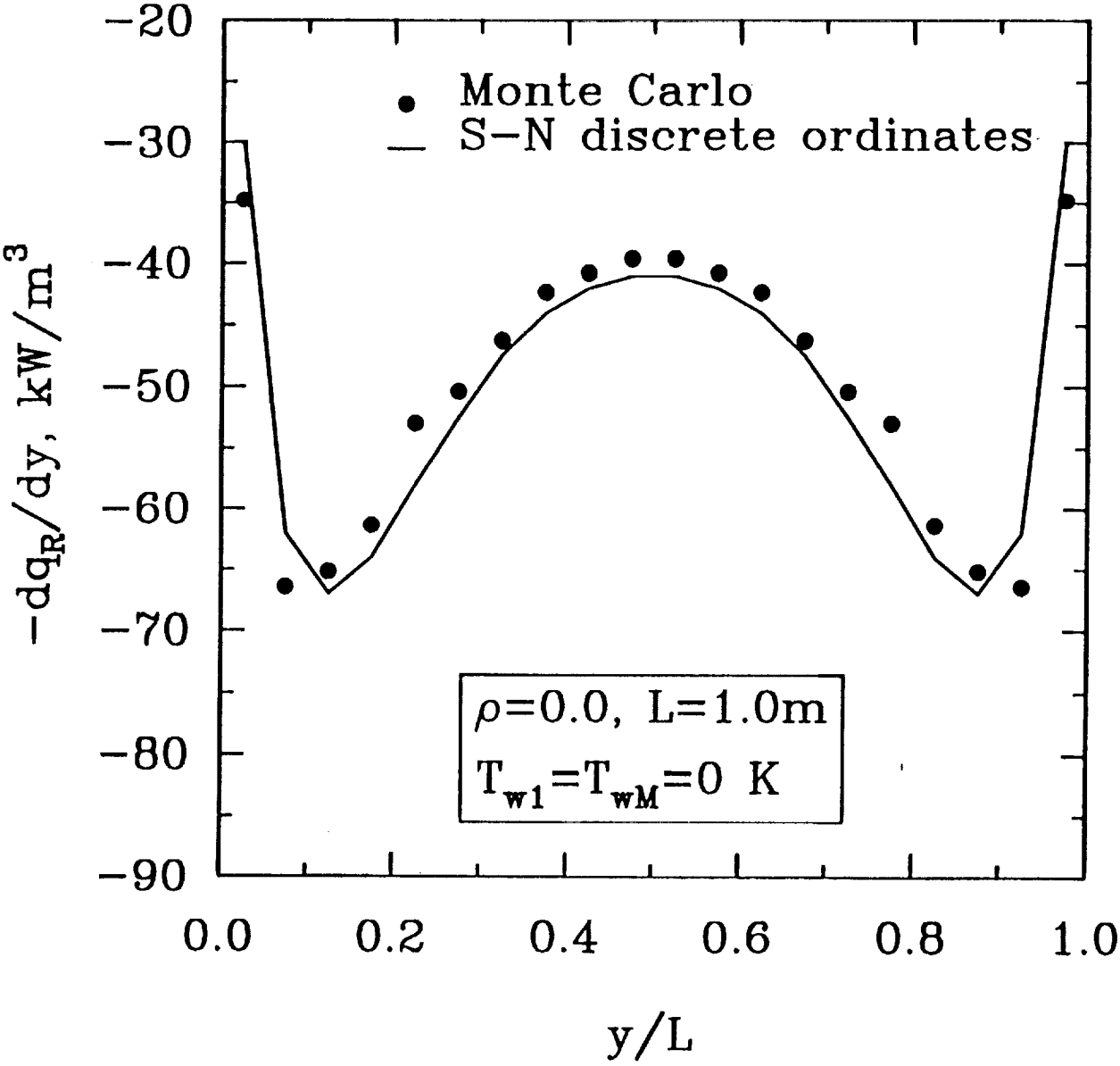

Fig. 3.3(d) Comparison of radiative dissipation for the parabolic H_2O concentration profile.

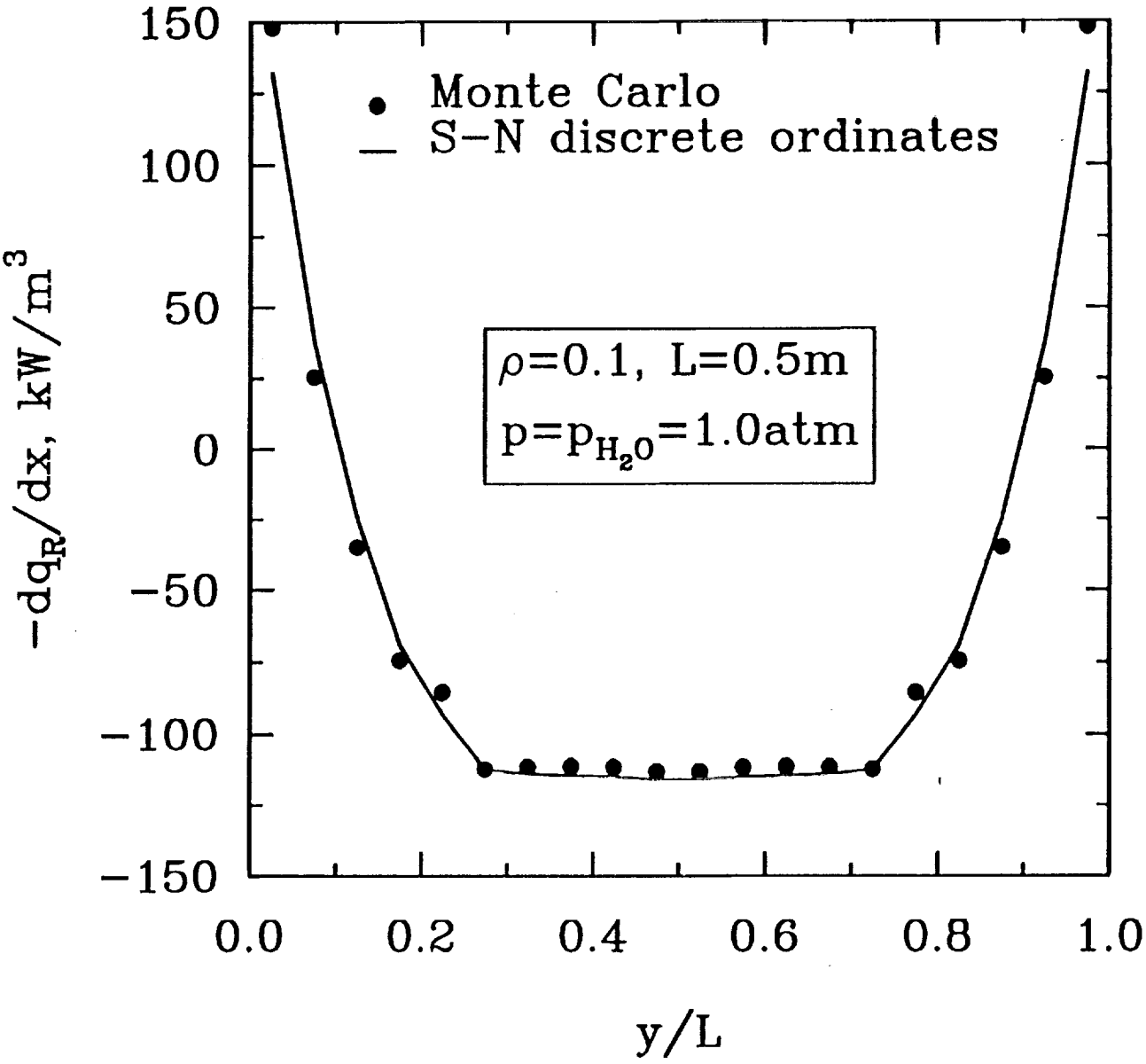

Fig. 3.4(a) Comparison of radiative dissipation in pure H_2O for ρ=0.1,L=0.5m.

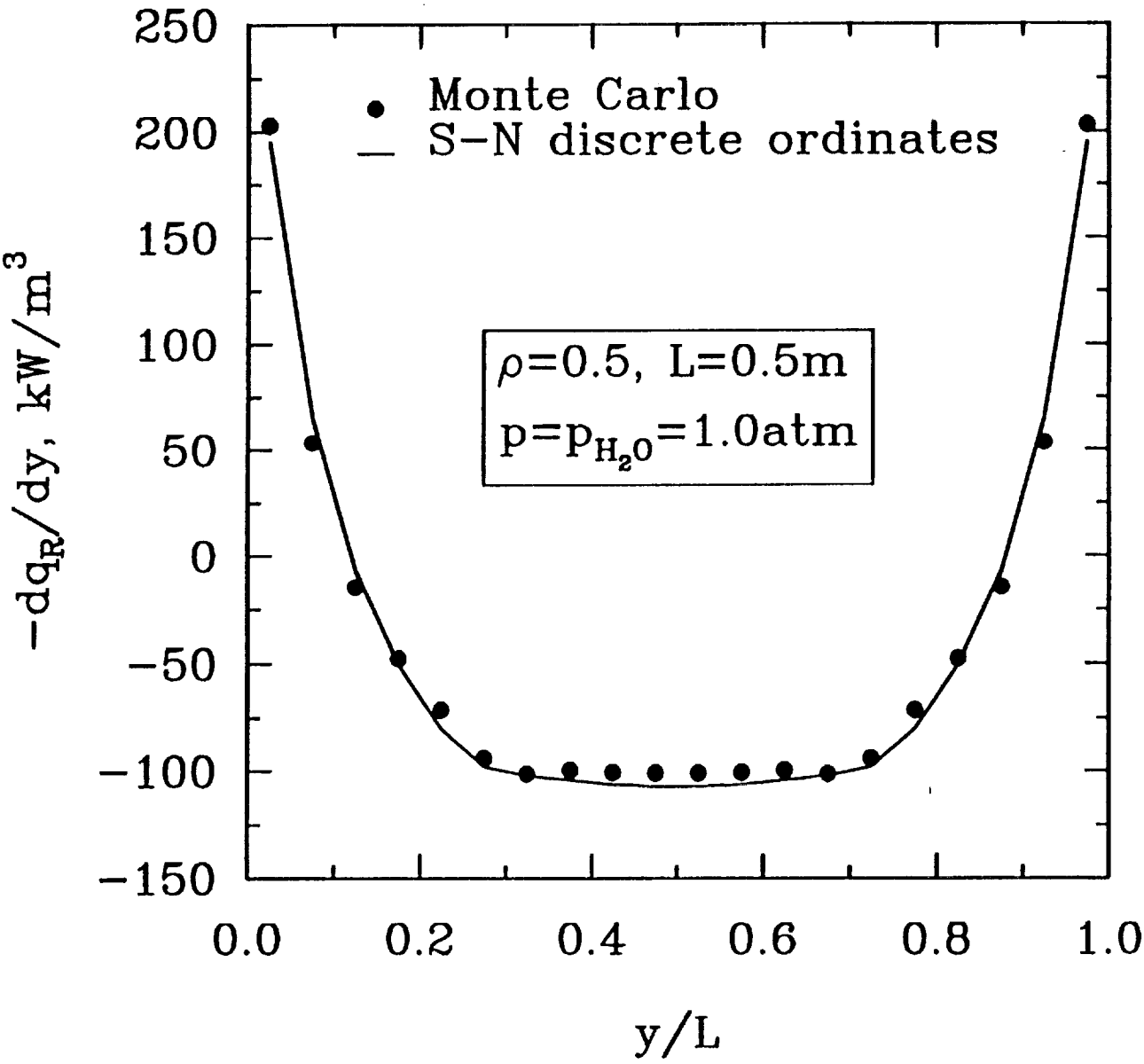

Fig. 3.4(b) Comparison of radiative dissipation in pure H_2O for ρ=0.5, L=0.5m.

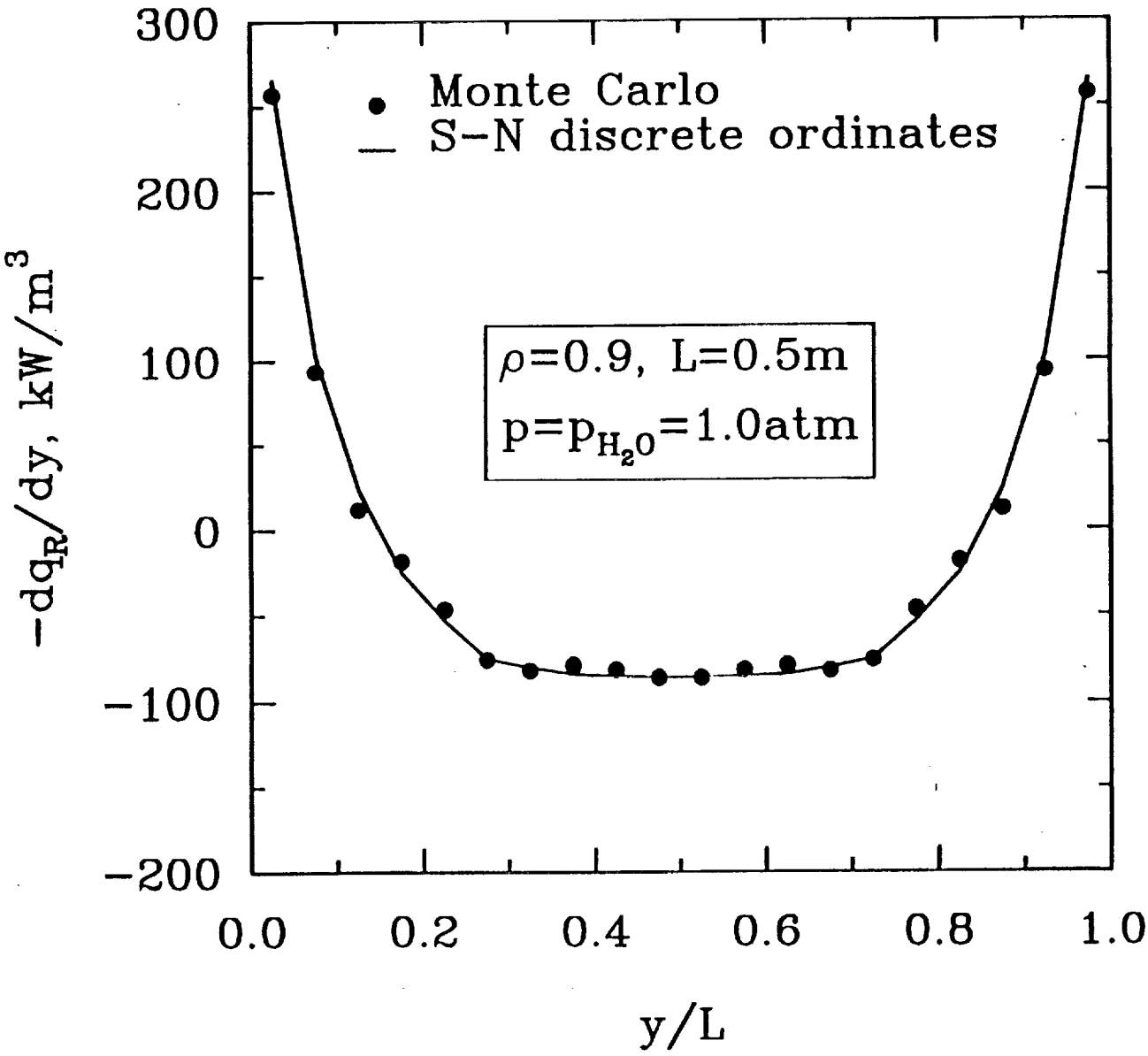

Fig. 3.4(c) Comparison of radiative dissipation in pure H_2O for ρ=0.9, L=0.5m.

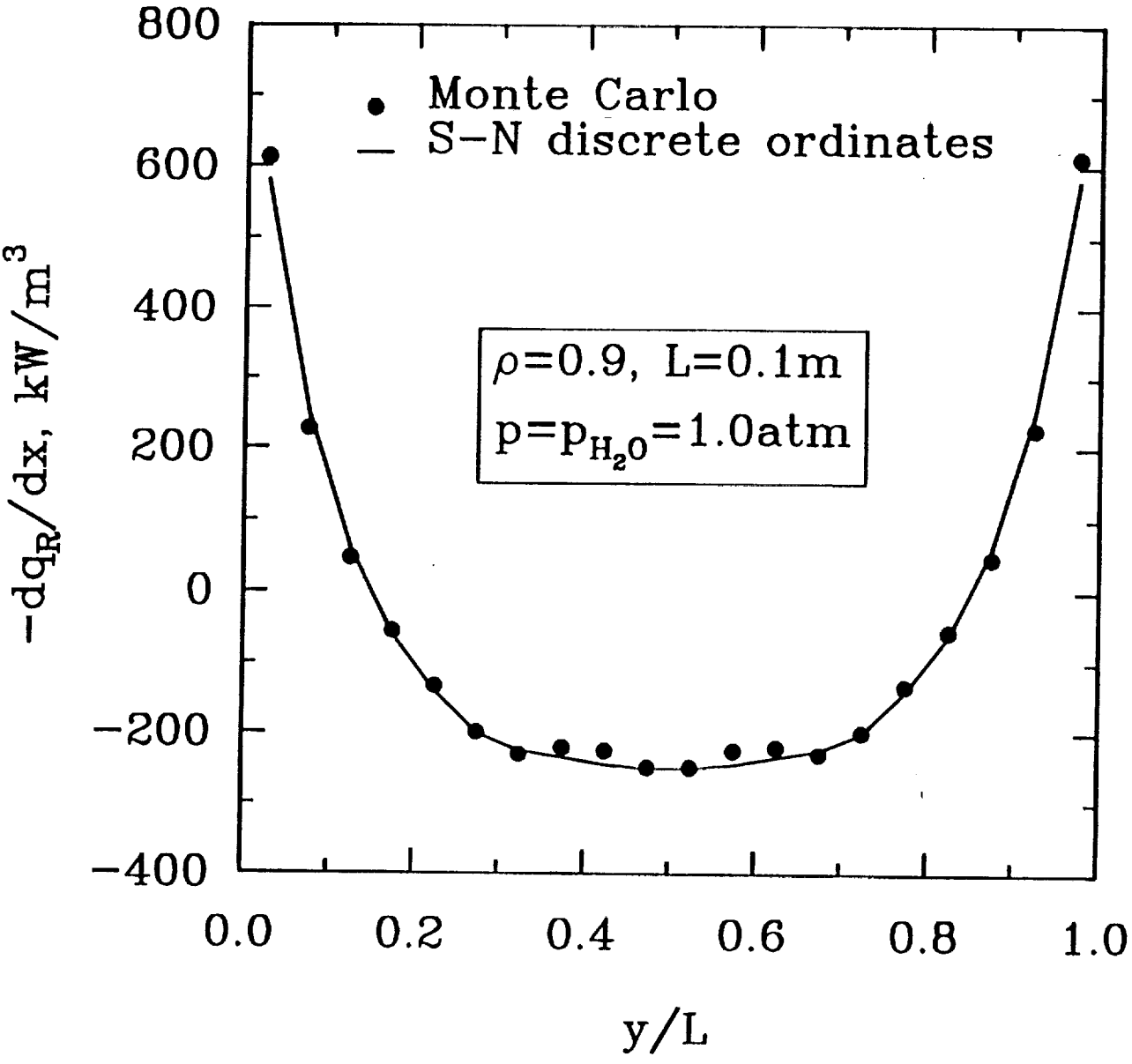

Fig. 3.4(d) Comparison of radiative dissipation in pure H_2O for ρ=0.9, L=0.1m.

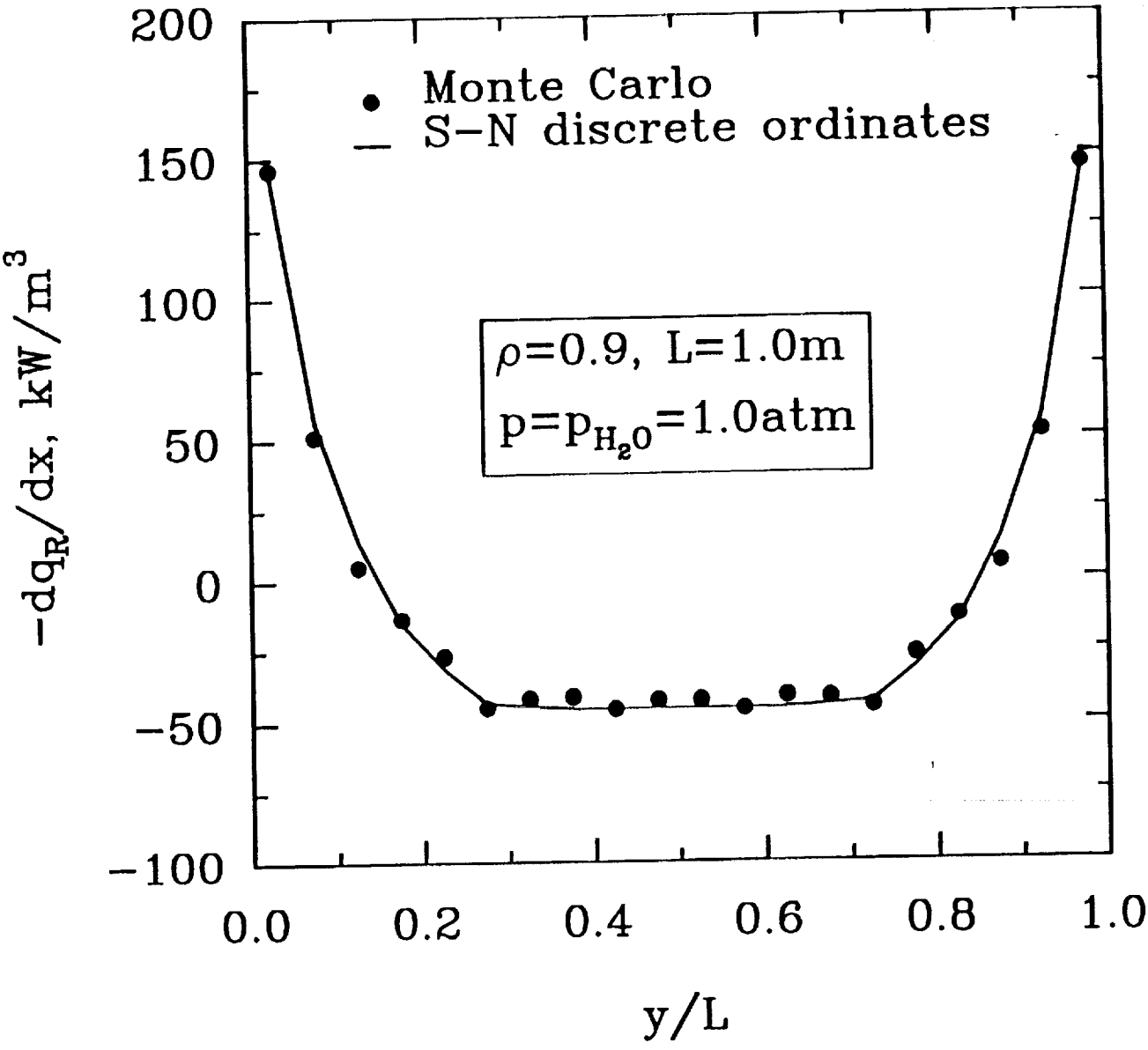

Fig. 3.4(e) Comparison of radiative dissipation in pure H_2O for ρ=0.9, L=1.0m.

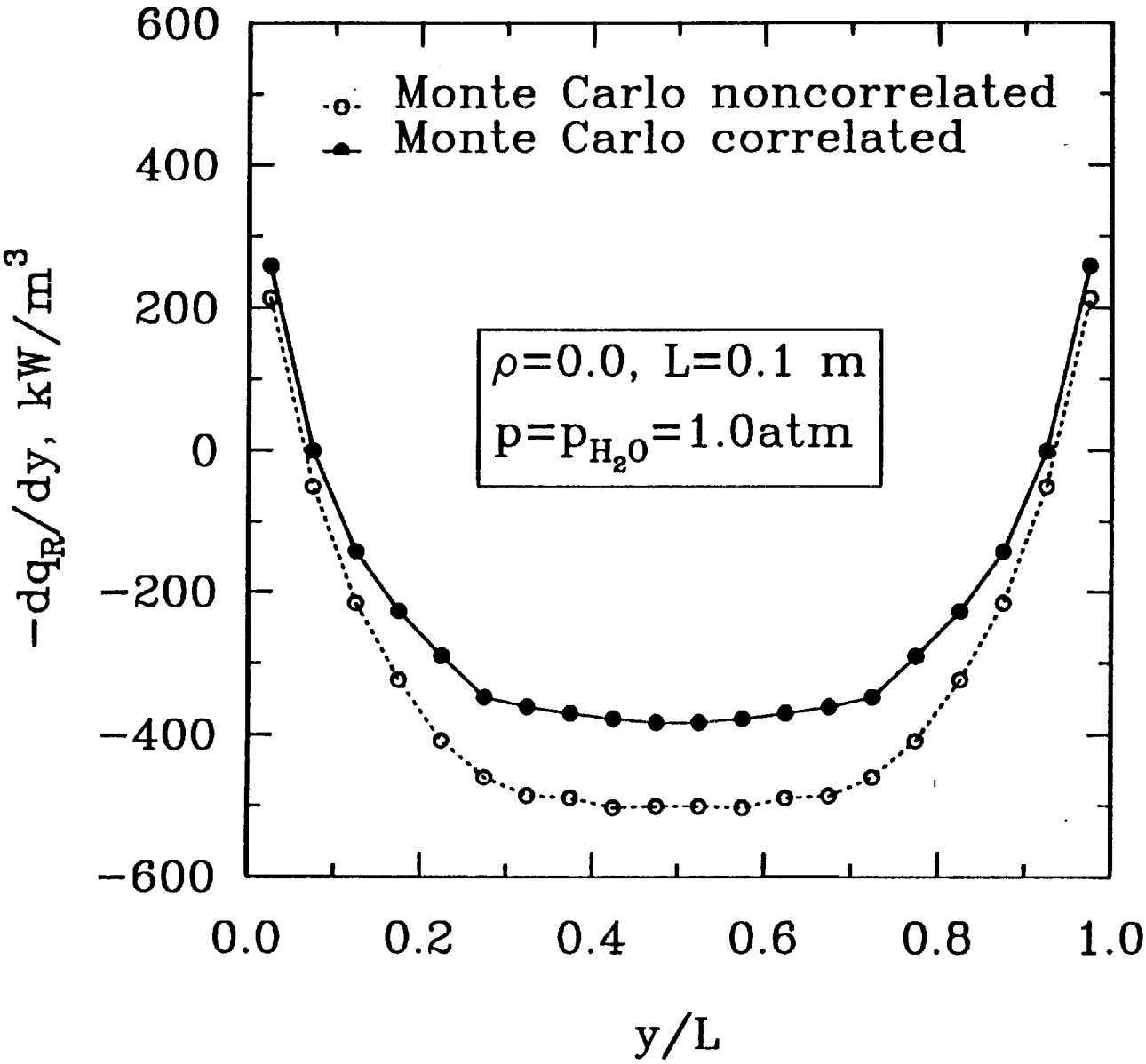

Fig. 3.5(a) Comparison of correlated and noncorrelated results in pure H_2O for ρ=0.0, L=0.1 m.

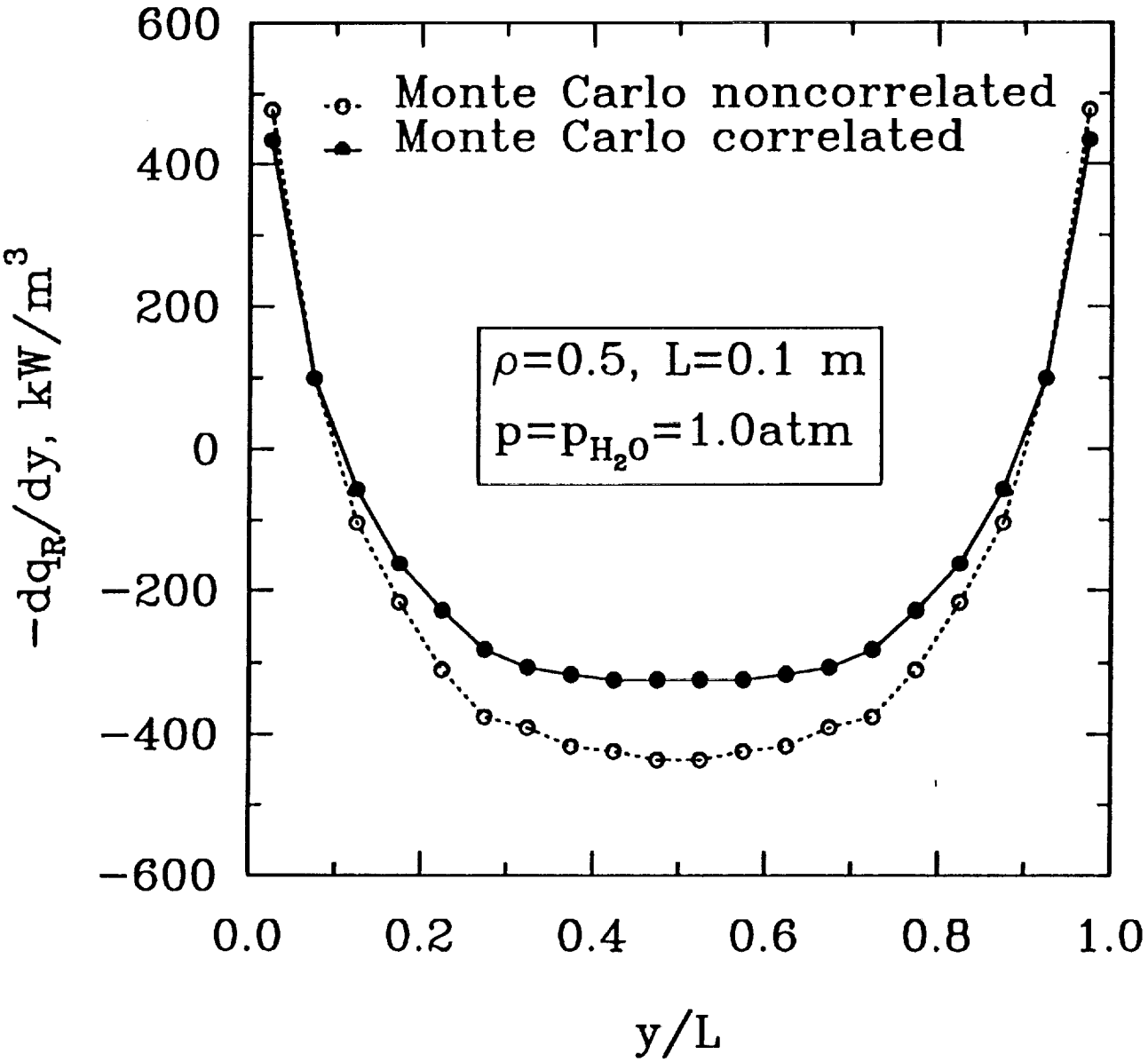

Fig. 3.5(b) Comparison of correlated and noncorrelated results in pure H_2O for ρ=0.5, L=0.1 m.

5. INVESTIGATION OF TWO-DIMENSIONAL RADIATION

In the previous sections, the MCM has been applied to investigate the radiative heat transfer in a one-dimensional problem with a nongray participating medium. When a narrow band model is employed, the spectral correlation between the transmittances of two different segments of the same path must be taken into account in the statistical relationship for determining the absorption location in order to get accurate results. For the nongray case with reflecting walls, the advantages of the MCM are very clear in comparison to other methods. Comparison of the Monte Carlo solutions with other solutions has justified the present Monte Carlo analysis.

The objective of this section is to extend the Monte Carlo analysis to a two-dimensional problem. Although it is well known that the MCM has a characteristics of easy extension of problem from one-dimensional to mutil-dimensional, a lot of difficulties may still exist and some unconventional treatments have to be applied during this extension. By considering a specific two-dimensional problem, some major difficulties encountered in a multi-dimensional problem will be handled in this section. A problem with any irregular geometry can be investigated in a similar way.

Consider an absorbing and emitting molecular gas between two parallel plates of finite length L and height H and infinite width as shown in Fig. 5.1. The inlet and outlet of the gas are at the section x=0 and x=L, respectively, and they are treated as pseudoblack walls with prescribed temperatures. Temperature, concentration and pressure in the medium are supposed to be known. The walls are assumed to be diffuse but not necessarily gray. The wall temperature distribution is also known. In order to calculate the net radiative wall flux and the radiative dissipation inside the medium, the medium considered is divided into an MX×MY array of rectangular volume elements (Fig. 5.1). Similarly, the two real walls are each divided into MX surface elements, and the inlet and outlet pesudo walls are each divided into MY surface elements. Temperature, concentration and pressure are assumed to be constant in each element.

The following Monte Carlo analyses are based on an arbitrarily chosen finite volume element ABCD (Fig. 5.2) with the length and height equal to b and c, respectively. Use of different assumptions results in three different sets of Monte Carlo formulations. They are the nongray narrow band formulations, approximate nongray narrow band formulations, and gray narrow band formulations, respectively. Investigation of differences of these formulations is another objective of this section.

5.1. Nongray Narrow Band Formulations

In this case, an energy bundle is simulated in an exact manner in terms of the narrow band model without any approximation. Let us consider the Planck spectral blackbody intensity $I_{b\omega}$ that enters the element ABCD at the point of s on the side of AB and intersects one of other three sides of the element at the point of s′ as shown in Fig. 5.2. It should be understood that each side of the element is a surface. A spherical coordinate system is established and centered at the point s. The distance between the points s and A is x^*. Under the condition of local thermodynamic equilibrium, an amount of energy absorbed in a finite volume element is equal to that emitted. Then, the amount of energy emitted for a wavenumber range $d\omega$ and a pencil of column s→s′ with a solid angle increment $d\Omega$ and an area increment dx^* is

$$dQ = I_{b\omega}\left[1 - \tau_\omega(s \rightarrow s')\right] \cos\theta d\Omega dx^* d\omega \tag{5.1}$$

The symbols in the above equation have the same meanings as the one-dimensional problem analyzed before. The total emitted energy calculated in terms of the intensity entering from the sides of AB ($0<\theta\leq\pi$) and DC ($\pi<\theta\leq 2\pi$) is obtained by integrating Eq. (5.1) over the wavenumber, polar angle, azimuthal angle and area as

$$Q = \int_0^\infty \int_0^b \int_0^\pi \int_0^{2\pi} I_{b\omega}\left[1 - \tau_\omega(s \rightarrow s')\right] \cos\theta \sin\theta d\psi d\theta dx^* d\omega \tag{5.2}$$

Referring to Fig. 5.2, the distance ss′ is expressed as

$$ss' = \begin{cases} \min\{c/\cos\theta, \quad (b-x^*)/(\cos\psi\sin\theta)\}, & -\pi/2 < \psi \leq \pi/2 \\ \min\{c/\cos\theta, \quad -x^*/(\cos\psi\sin\theta)\}, & \pi/2 < \psi \leq 3\pi/2 \end{cases} \tag{5.3}$$

The value of ss′cannot be calculated from just one expression because the point s′ may be located on the different sides of the element ABCD. All the possible travelling paths of the intensity in the element ABCD should be considered to evaluate the value of Q.

Similar procedures can be applied to obtain the expression for the emitted radiative energy calculated in terms of the intensity entering from the sides of AD and BC. Then the total emitted radiative energy from the finite volume element ABCD consists of two terms. They represent the emitted energy calculated in terms of the intensities entering from the sides of AB, DC and the sides of AD, BC, respectively, and cannot be manipulated algebraically into one term. Usually, the statistical relationships for simulating an energy bundle emitted from a volume element in the MCM are developed from the formulation of total emitted radiative energy of this volume element. But this may complicate the analysis for a multi-dimensional problem since there exist two or even more independent terms in the formulation of total emitted radiative energy. In this study, the two independent terms in the present problem are treated separately, and the Monte Carlo analysis is based on a single term. This means that the Monte Carlo analysis is based on Eq. (5.2) if an energy bundle in the element ABCD starts from the sides of AB or DC. Otherwise, the Monte Carlo analysis is from another term. The following Monte Carlo formulations are developed based on Eq. (5.2), and the Monte Carlo formulations from another term can be derived in the same way.

The simulation of an energy bundle includes the determination of wavenumber, point of emission and direction of emission of this energy bundle in the finite volume element. The statistical relationships for determining these parameters are readily obtained from Eq. (5.2) as (Howell, 1968; Siegel and Howell, 1981; Haji-Sheikh, 1988)

$$R_\omega = \frac{\int_0^\omega \int_0^b \int_0^\pi \int_0^{2\pi} I_{b\omega}[1 - \tau_\omega(s \rightarrow s')] \cos\theta \sin\theta d\psi d\theta dx^* d\omega}{Q} \tag{5.4}$$

$$R_{x^*} = \frac{\int_0^{x^*} \int_0^\infty \int_0^\pi \int_0^{2\pi} I_{b\omega}[1 - \tau_\omega(s \rightarrow s')] \cos\theta \sin\theta d\psi d\theta d\omega dx^*}{Q} \tag{5.5}$$

$$R_\theta = \frac{\int_0^\theta \int_0^\infty \int_0^b \int_0^{2\pi} I_{b\omega}[1-\tau_\omega(s\rightarrow s')]\cos\theta\sin\theta d\psi dx^* d\omega d\theta}{Q} \tag{5.6}$$

$$R_\psi = \frac{\int_0^\psi \int_0^\infty \int_0^b \int_0^{\pi} I_{b\omega}[1-\tau_\omega(s\rightarrow s')]\cos\theta\sin\theta d\theta dx^* d\omega d\psi}{Q} \tag{5.7}$$

where $R_\omega, R_{x^*}, R_\theta, R_\psi$ are random numbers which are uniformly distributed between zero and one. In Eqs. (5.2) and (5.4)-(5.7), τ_ω is a real spectral transmittance. Before solving these equations to obtain ω, x^*, θ and ψ from a set of given values of $R_\omega, R_{x^*}, R_\theta, R_\psi$, the narrow band model should be applied to approximate the real spectral transmittance.

Taking the spectral average over all narrow bands and using the narrow band approximation as that in Eq. (3.8), Eqs. (5.2) and (5.4)-(5.7) are expressed as

$$Q = \sum_{k=1}^{m_\omega} \left\{ \int_0^b \int_0^\pi \int_0^{2\pi} \overline{I_{b\omega^k}}[1-\overline{\tau_{\omega^k}}(s\rightarrow s')]\cos\theta\sin\theta d\psi d\theta dx^* \right\} \Delta\omega^k \tag{5.8}$$

$$R_\omega = \frac{\sum_{k=1}^{n} \left\{ \int_0^b \int_0^\pi \int_0^{2\pi} \overline{I_{b\omega^k}}[1-\overline{\tau_{\omega^k}}(s\rightarrow s')]\cos\theta\sin\theta d\psi d\theta dx^* \right\} \Delta\omega^k}{Q}, \quad (\omega^{n-1} < \omega \le \omega^n) \tag{5.9}$$

$$R_{x^*} = \frac{\sum_{k=1}^{m_\omega} \left\{ \int_0^{x^*} \int_0^\pi \int_0^{2\pi} \overline{I_{b\omega^k}}[1-\overline{\tau_{\omega^k}}(s\rightarrow s')]\cos\theta\sin\theta d\psi d\theta dx^* \right\} \Delta\omega^k}{Q} \tag{5.10}$$

$$R_\theta = \frac{\sum_{k=1}^{m_\omega} \left\{ \int_0^\theta \int_0^b \int_0^{2\pi} \overline{I_{b\omega^k}}[1-\overline{\tau_{\omega^k}}(s\rightarrow s')]\cos\theta\sin\theta d\psi dx^* d\theta \right\} \Delta\omega^k}{Q} \tag{5.11}$$

$$R_\psi = \frac{\sum_{k=1}^{m_\omega} \left\{ \int_0^\psi \int_0^b \int_0^{\pi} \overline{I_{b\omega^k}}[1-\overline{\tau_{\omega^k}}(s\rightarrow s')]\cos\theta\sin\theta d\theta dx^* d\psi \right\} \Delta\omega^k}{Q} \tag{5.12}$$

where m_ω is the total number of narrow bands. Similar to one-dimensional problem, in order to solve Eqs. (5.9)-(5.12) for a set of given values of R_ω, R_{x^*}, R_θ and R_ψ, interpolation and approximation methods have to be employed.

The integrations involved in Eqs. (5.8)-(5.12) need to be evaluated numerically. First, each integration variable should be discretized within its range. The wavenumber in Eqs. (5.8)-(5.12) has been already divided into m_ω narrow bands. Similarly, the side length is divided into m_{x^*} elements between 0 to b; the polar angle is divided into m_θ elements between 0 to π; the azimuthal angle is divided into m_ψ elements between 0 to 2π. The value in each element of a variable is assumed to be constant. Then, by drawing a value from each variable, a pencil of medium column is determined and the emitted radiative energy of this column is calculated from the integrand in Eq. (5.8). If all the combination of four values from four different variables are taken into account, an array ($m_\omega \times m_{x^*} \times m_\theta \times m_\psi$) is obtained in which the value of each array element represents the emitted radiative energy of a medium column. The total emitted radiative energy Q is equal to the summation of values of all the elements in the array. The integrations involved in Eqs. (5.9)-(5.12) are equal to the summation of values of part of elements in the array. As a matter of fact, the variable x^*, θ and ψ only need to be discretized within the half of their ranges because of the symmetry of transmitting of intensity in a rectangular finite volume element. This symmetry saves the storage space and reduces the computer time considerably in the numerical integration.

To determine the location of absorption of the energy bundle in the participating medium, let us still consider the emitted radiant energy along a pencil of column s→s′ (Fig. 5.1). After this amount of energy is transmitted over a column s′→s″, the remaining radiant energy is given by

$$dQ' = I_{b\omega}\left[1 - \tau_\omega(s \to s')\right]\tau_\omega(s' \to s'')\cos\theta d\Omega dx^* d\omega \tag{5.13}$$

Taking a narrow band average over Eqs. (5.1) and (5.13) and dividing the latter one with the first one, we obtain the same the statistical relationship for determining the location of absorption as that for one-dimensional problem,

$$R_l = \frac{\overline{\tau_\omega}(s' \to s'') - \overline{\tau_\omega}(s \to s'')}{1 - \overline{\tau_\omega}(s \to s')} \tag{5.14}$$

5.2. Gray Narrow Band Formulations

For gray formulations, the radiative properties are assumed to be constant in a narrow band. The correlation between various spectrally dependent quantities no longer exists. So there is only one statistical relationship in this case which is different from the nongray narrow band. This different relationship is the statistical relationship for determining the location of absorption and it has the same formulation as Eq. (3.12). From the previous analysis, the R_I calculated from the case of gray narrow band is greater than the case of nongray narrow band.

5.3. Approximate Nongray Narrow Band Formulations

In this case, the volume dV of a volume element is assumed to be very small so that energy emitted within dV escapes before reabsorption within dV. This has been the basic assumption employed in all the studies related to the MCM so far. In fact, this assumption is applied in most works no matter whether or not it is really satisfied. Major advantage of this assumption is that radiative transfer formulations can be simplified significantly. From Howell (1968) and Siegal and Howell (1981), the total emitted radiative energy and the statistical relationships for determining the wavenumber and emission direction of an energy bundle emitted from a finite volume dV are given by

$$Q_{dV} = 4\pi \int_0^\infty \kappa_\omega I_{b\omega} dV\, d\omega \tag{5.15}$$

$$R_\omega = \frac{\int_0^\omega \kappa_\omega I_{b\omega} d\omega}{\int_0^\infty \kappa_\omega I_{b\omega} d\omega} \tag{5.16}$$

$$R_\theta = \frac{1 - \cos\theta}{2} \tag{5.17}$$

$$R_\psi = \frac{\psi}{2\pi} \tag{5.18}$$

where κ_ω is the spectral absorption coefficient. The location of emission of an energy bundle is determined in such a way that all the energy bundles are assumed to pass the center point of the element. This treatment is justified from the assumption used in the case considered. Introducing the narrow band approximation, Eqs. (5.15) and (5.16) becomes

$$Q_{dV} = 4\pi \sum_{k=1}^{m_\omega} \left(\overline{\kappa_{\omega^k}} \overline{I_{b\omega^k}} \Delta\omega^k \right) dV \tag{5.19}$$

$$R_\omega = \frac{4\pi \sum_{k=1}^{n} \left(\overline{\kappa_{\omega^k}} \overline{I_{b\omega^k}} \Delta\omega^k \right) dV}{Q_{dV}}, \qquad \left(\omega^{n-1} < \omega \leq \omega^n \right) \tag{5.20}$$

The term $\overline{\kappa_{\omega^k}}$ is the mean absorption coefficient over a narrow band and is obtained as (Kim et al., 1991a)

$$\overline{\kappa_{\omega^k}} \simeq -\frac{\ln \overline{\tau_{\omega^k}}(L_{MB})}{L_{MB}} \tag{5.21}$$

where L_{MB} is the mean beam length of the volume element. It is evident that Eqs. (5.17)-(5.20) are much simpler than the corresponding formulations for the cases of nongray and gray narrow bands.

The statistical relationship for determining the location of absorption of an energy bundle emitted from the volume element dV should be treated in a different way from that in Howell (1968) and Siegal and Howell (1981) in this case because of the incorporation of a narrow band model. Equation (5.14) is the general formulation to calculate R_l with consideration of the spectral correlation. Substituting the mean transmittances with the mean absorption coefficients, Eq. (5.14) becomes

$$R_l = \frac{\exp\left(-\int_{s'}^{s''} \overline{\kappa_\omega} ds \right) - \exp\left(-\int_{s}^{s''} \overline{\kappa_\omega} ds \right)}{1 - \exp\left(-\int_{s}^{s'} \overline{\kappa_\omega} ds \right)} \tag{5.22}$$

Since dV is very small, we have the following approximation

$$1 - \exp\left(-\int_{s}^{s'} \overline{\kappa_\omega} ds \right) \approx \overline{\kappa_\omega} s s' \tag{5.23}$$

This approximation is also applied in deriving Eqs. (5.15)-(5.18). Equation (5.22) is then simplified as

$$R_l = \frac{\exp\left(-\int_{s'}^{s''} \overline{\kappa_\omega} ds\right) - \exp\left(-\int_{s}^{s''} \overline{\kappa_\omega} ds\right)}{\overline{\kappa_\omega} ss'} \tag{5.24}$$

Equation (5.24) is also quite different from the statistical relationship usually employed for determining the location of absorption in the Monte Carlo simulation. Like the case of the gray narrow band, the R_l calculated from Eq. (5.24) is usually greater than that calculated from Eq. (5.14) for the same conditions because of use of the approximations given in Eqs. (5.21) and (5.23). An alternative way to obtain Eq. (5.24) is to follow the same procedures as those in the case of nongray narrow band for determining R_l and apply the required approximation at the very beginning of the derivation.

5.4. Results and Discussions

Based on the Monte Carlo analyses described in the previous section, a computer code is developed that is able to predict the radiative dissipation and net radiative wall flux using a narrow band model in a nonisothermal and inhomogeneous medium. The calculations are carried out for two different temperature distributions with a uniform composition of pure H_2O vapor at 1 atm using a Sun Workstation. The narrow band calculation goes up to 4250 cm^{-1} for H_2O and the total number of narrow bands considered is m_ω=165. For the uniform temperature distribution, the gas temperature is chosen to be 1000 K, while the real and pseudo walls are held at 0 K. The two real wall emissivities are assumed to be same and equal to 0.5. Three cases with different aspect ratios (=L/H) are investigated for this temperature distribution. For the nonuniform temperature distribution, the gas temperature is assumed to be

$$T(x,y) = 800 + 700\left[1 - \frac{|\,2y - H\,|}{H}\right]\frac{x}{L} \tag{5.25}$$

The two real walls and the inlet pseudo wall are kept at a temperature of 800 K. The outlet of the gas is open to a 300 K atmosphere, so the temperature of the outlet pseudo wall is at 300 K.

The two real wall emissivities are chosen to be same and equal to 0.6. The length and height of two parallel plates are 0.6 m and 0.3 m, respectively. This is the only one geometrical size considered in this situation. The work from Zhang et al. (1988) has been referred to construct the wall and geometrical conditions in the case of nonuniform temperature distribution.

In the Monte Carlo simulation, the medium is divided into 20×20 uniform finite volume elements for all calculations. Subsequently, the number of finite surface elements on each wall is 20. Further subdivision of the computation domain yields little changes in the results. For integrations and interpolations in the nongray and gray narrow band formulations, the divisions of the side length, polar angle and azimuthal angle in a rectangular volume element are chosen to be $m_{x'}=10$, $m_\theta=10$ and $m_\psi=10$ respectively within half of their ranges. The emitted radiative energy from each of the $m_\omega \times m_{x'} \times m_\theta \times m_\psi = 165\times 10\times 10\times 10$ medium columns is then calculated and stored. The required integrations and interpolations are implemented from the summation of the values of radiative energy in different columns. These computations should be done for each volume element in the case of nonuniform temperature distribution because the integrations and interpolations values evaluated in one volume element are different from another volume element due to the temperature differences. Obviously this work will be very time-consuming. Similar probelm will be encounteded in other multi-dimensional problems. In this stusy, a temperature interpolation technique has been developed to reduce the computer time. We make the integrations and interpolations in Eqs. (5.8)-(5.12) at 15 different temperatures which are uniformly distributed within the temperature range in the medium. The values of the required integrations and interpolations in each of volume elements can be interpolated from the results at these 15 different temperatures by using B-spline functions. Care should be taken to choose the number of temperature interpolation points. Too small number may not result in accurate results.

The total number of energy bundles for all cases is chosen to be 500,000. This choice represents a compromise between accuracy and saving of computation time. Numerical experiments has been done for different Monte Carlo solutions and indicate that an increase in the total number of energy bundles by a factor of 10 results in a change in the least squares fit of

the Monte Carlo results not more than ±2%; but the computing time increases by a factor of 10. The CPU times required for the nongray (narrow band) solution and gray (narrow band) solution are about the same. They are about 20–25 minutes for the case of uniform temperature distribution and 35–40 minutes for the case of nonuniform temperature distribution. If the temperature interpolation technique is not applied, the CPU time mentioned previously in the nonuniform temperature case is increased by a factor of 7–10 to get almost the same results. The approximate nongray (narrow band) solution does not need to use a temperature interpolation technique and takes less CPU time to complete than the nongray and gray solutions. However, the time difference is not more than five minutes in each case.

Besides the three above mentioned solutions, one-dimensional nongray (narrow band) results are also obtained in each case for comparison. The formulations of one-dimensional problem have been given in the section 3. In the one-dimensional nongray solution, the radiative heat transfer is simulated in an exact manner like that for the nongray solution. But it is only dependent on the temperature distribution at one x location, while the other three two-dimensional solutions are dependent on the temperature distribution over the entire computational domain. Among the four different solutions, the nongray solution is the most accurate and is used to compare the other solutions. Also, the Monte Carlo results tend to show little fluctuations around the "real" answers. A least squares method has been applied to fit the fluctuated results in all the four solutions obtained in this study.

The situation with uniform temperature distribution is considered first. The behaviors of four different narrow band solutions are illustrated in Figs. 5.3(a)-5.3(f) for three cases with different aspect ratios. The height of the plates is assumed to be constant and equal to H=0.1 m. Different values of aspect ratio are obtained by changing the length of the plates. Figures 5.3(a)–5.3(c) show the distribution of radiative dissipation at the middle location of the plates with aspect ratio equal to one, four and ten, respectively. One-dimensional nongray solution is identical for all the three cases, while the three two-dimensional solutions are different. For the case with small aspect ratio in Fig. 5.3(a), the one-dimensional nongray solution is well above the nongray

solution. The radiative energy absorbed in the medium from the one-dimensional treatment is much higher than that from the two-dimensional treatment. Among the three two-dimensional solutions, the approximate nongray solution falls approximately 20–25% below the nongray solution. The gray solution falls even more, 50–60% below the nongray solution. As the aspect ratio increases to four in Fig. 5.3(b), more radiative energy is absorbed in the medium at the middle location. So values of radiative dissipation from nongray solution increase and approach the one-dimensional nongray solution. The approximate nongray results and gray results also increase in this case; but they still overpredict the emission of radiative energy. When the aspect ratio is further increased to ten in Fig. 5.3(c), the nongray results are increased to their limiting values which are nothing but one-dimensional nongray results. It seems that the approximate nongray solution and gray solution also reach to their own limiting values that are about 20% and 70% below the nongray results, respectively.

The distribution of radiative wall flux along the parallel plates for the cases presented in Figs. 5.3(a)-5.3(c) are shown in Figs. 5.3(d)-5.3(e). The one-dimensional nongray result is a constant value along the plates which is the same for the three cases. In Fig. 5.3(d), the length of the plates is equal to the height. Similar to the radiative dissipation case, the one-dimensional nongray solution and nongray solution differ significantly. More energy is absorbed on the plates for the one-dimensional treatment as compared to the two-dimensional treatment. Significant differences are also noted among the three two-dimensional solutions. The approximate nongray solution and gray solution overestimate the energy absorbed on the walls by about 20% and 40%, respectively, as compared to the nongray solution. In Fig. 5.3(e), the aspect ratio is increased to four. The radiative wall flux predicted by the three two-dimensional solutions also increase. When the aspect ratio becomes ten in Fig. 5.3(f), except the ranges near the inlet and outlet, the nongray solution reaches to a plateau of uniform radiative wall flux in the central region. The value of the plateau exactly matches the one-dimensional nongray result. The results from the approximate nongray solution and gray solution show a trend similar to that of the nongray solution. However, the plateau values in the central region are about 15% and 50% higher than

the nongray solution, respectively.

From the results presented in Figs. 5.3(a)-5.3(f), it is evident that the two-dimensional effects are dominant in the entire domain for the parallel plates with a small aspect ratio, while the one-dimensional effects are dominant for the parallel plates with a large aspect ratio. In the inlet and outlet regions, the two-dimensional effects are always important no matter what the aspect ratio is chosen. Among the three two-dimensional solutions, the approximate nongray solution and gray solution predict a lower distribution of radiative dissipation in the middle location and higher radiative wall fluxes along the plates than the nongray solution. There are physical justifications for these discrepancies. As indicated in the previous section, the Re_l calculated from the nongray formulation is smaller than that calculated from the approximate nongray formulation. So an energy bundle travels a short distance and is likely to be absorbed in the region near the point of emission. In the approximate nongray solution, however, an energy bundle travels a long distance which may be several times larger than the height of the plates and is more likely to be absorbed on the walls. The gray formulation predicts even longer travelling distance of an energy bundle than the approximate nongray formulation. This is why the differences between the gray solution and nongray solution are larger than those between the approximate nongray solution and nongray solution.

The situation with the nonunifrom temperature distribution is considered next. The temperature in the medium calculated from Eq. (5.25) is observed to increase as the distance from the walls and the inlet increase. Figures 5.4(a)-5.4(c) show the distributions of the radiative dissipation at three different locations along the plates. In Fig. 5.4(a), the location is chosen to be near the inlet (x/L=0.275) where temperature change is quite smooth. In this case, the travelling distance of an energy bundle predicted from the approximate nongray formulation is about the same as the height of the plates, and an energy bundle is more likely to be absorbed near and on the walls. Thus, it is observed that the approximate nongray results are higher than the nongray results in the region near the walls but lower in the central region. Similar trend is also found for the one-dimensional nongray solution. Unlike the approximate nongray formulation, the gray

formulation still predicts a much larger travelling distance of an energy bundle than the height of the plates. Therefore, the gray solution is much lower than the nongray solution in the entire region. Figure 5.4(b) shows the results at the location x/L=0.575. The one-dimensional nongray solution tends to be a little separated from the three two-dimensional solutions. The differences among the three two-dimensional solutions are similar to the previous case. In Fig. 5.4(c), the location is chosen to be near the outlet (x/L=0.875). The temperature change is steep and temperature values in the central region are high in this case. The one-dimensional nongray solution neglects the existence of the cold medium and cold walls around the location, and predicts more energy absorbed in the medium than other solutions. This is why the one-dimensional solution is significantly highter than the other three two-dimensional solutions. A little change is also found for the approximate nongray solution. The range where the approximate nongray results are lower than the nongray results has expanded to the place near the walls. It is believed that the steep change in temperature and high temperature values contribute to this phenomena. For the gray solution, it is still significantly below the nongray solution like the previous cases.

The distribution of radiative wall flux along the plates in the case of nonuniform temperature profile is presented in Fig. 5.4(d). As the location changes from the inlet to the outlet, the one-dimensional nongray results increase all the way, while the three two-dimensional results increase at first, reach a peak value at a place near the outlet, and then decrease. The reason for such behaviors between one-dimensional and two-dimensional treatments is obvious. The outlet region, in this problem, is equivalent to a cold source. This cold source has a strong effect on the radiative heat transfer in the nearby region. Two-dimensional solutions can predict this effect. But one-dimensional solution only depends the local temperature and is not exposed to the effect of the cold source. Among the three two-dimensional solutions, the gray results overestimate the energy absorbed on the walls by as much as a factor of two to five compared to the nongray results. This is compatible with the results of radiative dissipation presented in Figs. 5.4(a)-5.4(c). Similar to the previous cases, the approximate nongray solution is observed to be closer to the nongray solution. The maximum differences between these two solutions

occur in the location near the outlet and these are usually not more than 50%.

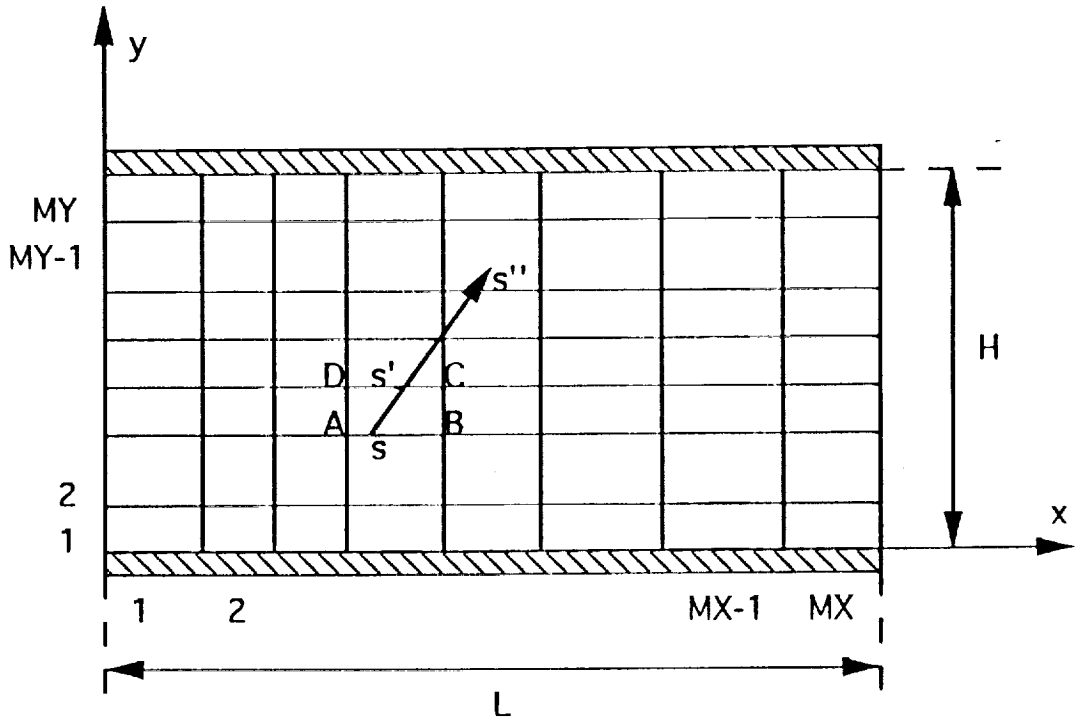

Fig. 5.1 Schematic of two finite parallel plates and grid configuration

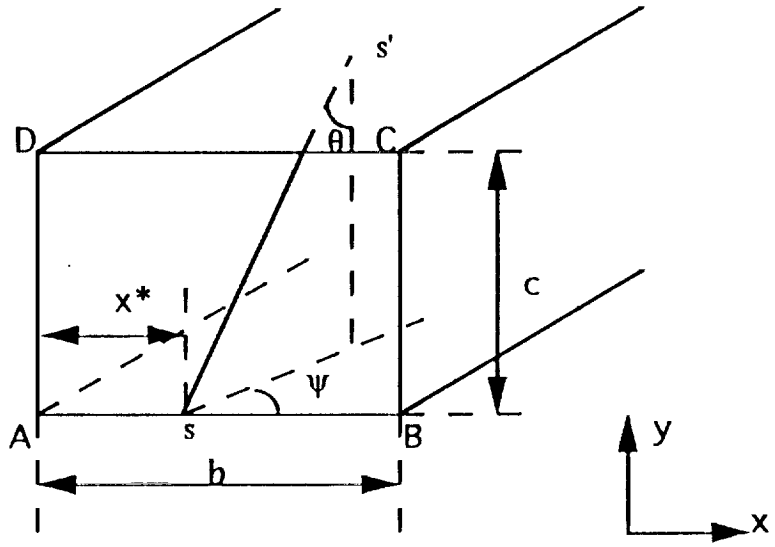

Fig. 5.2 Schematic of a rectangular finite volume element ABCD

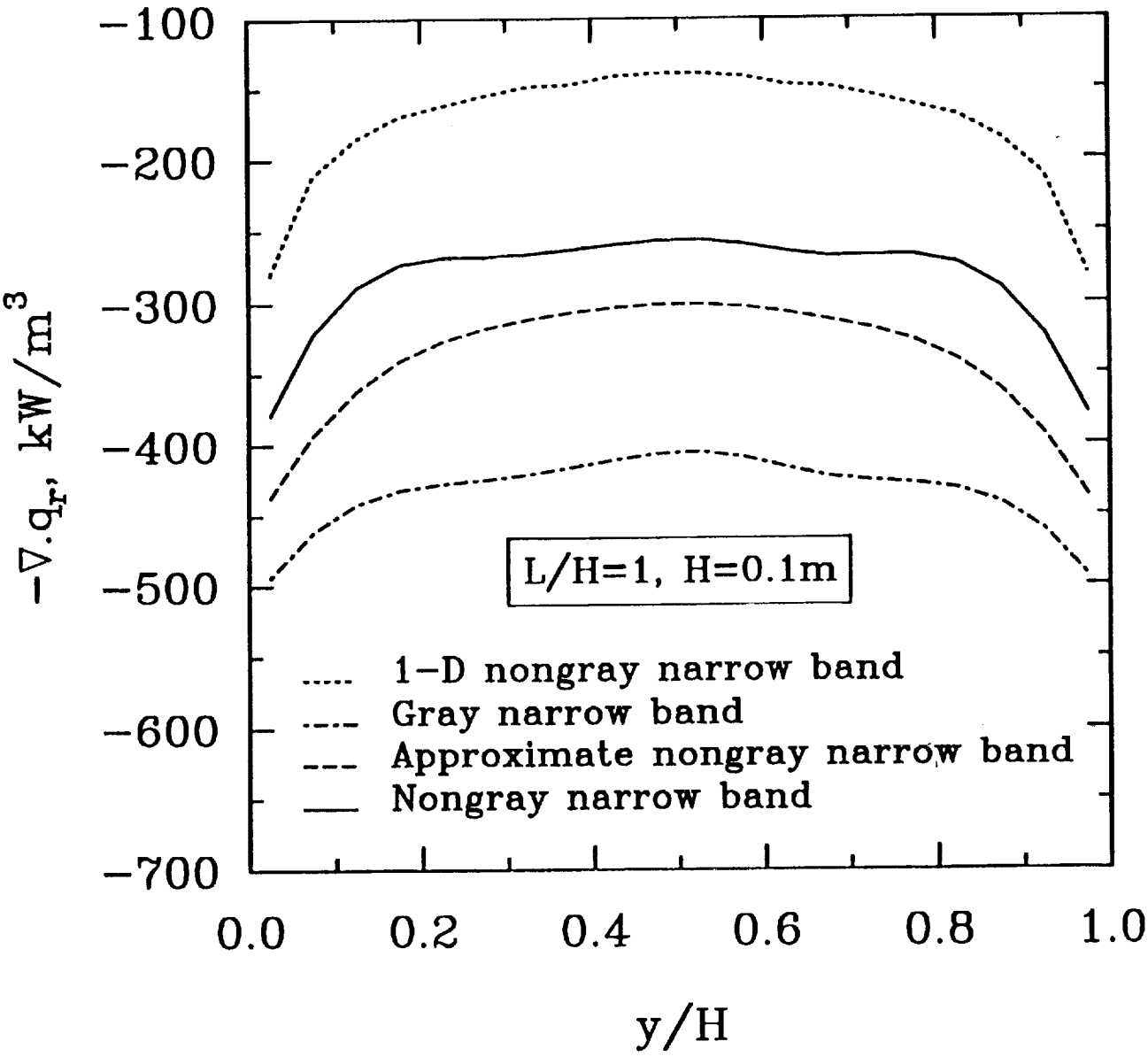

Fig. 5.3(a) Radiative dissipation at middle location for the case of uniform temperature (L/H=1).

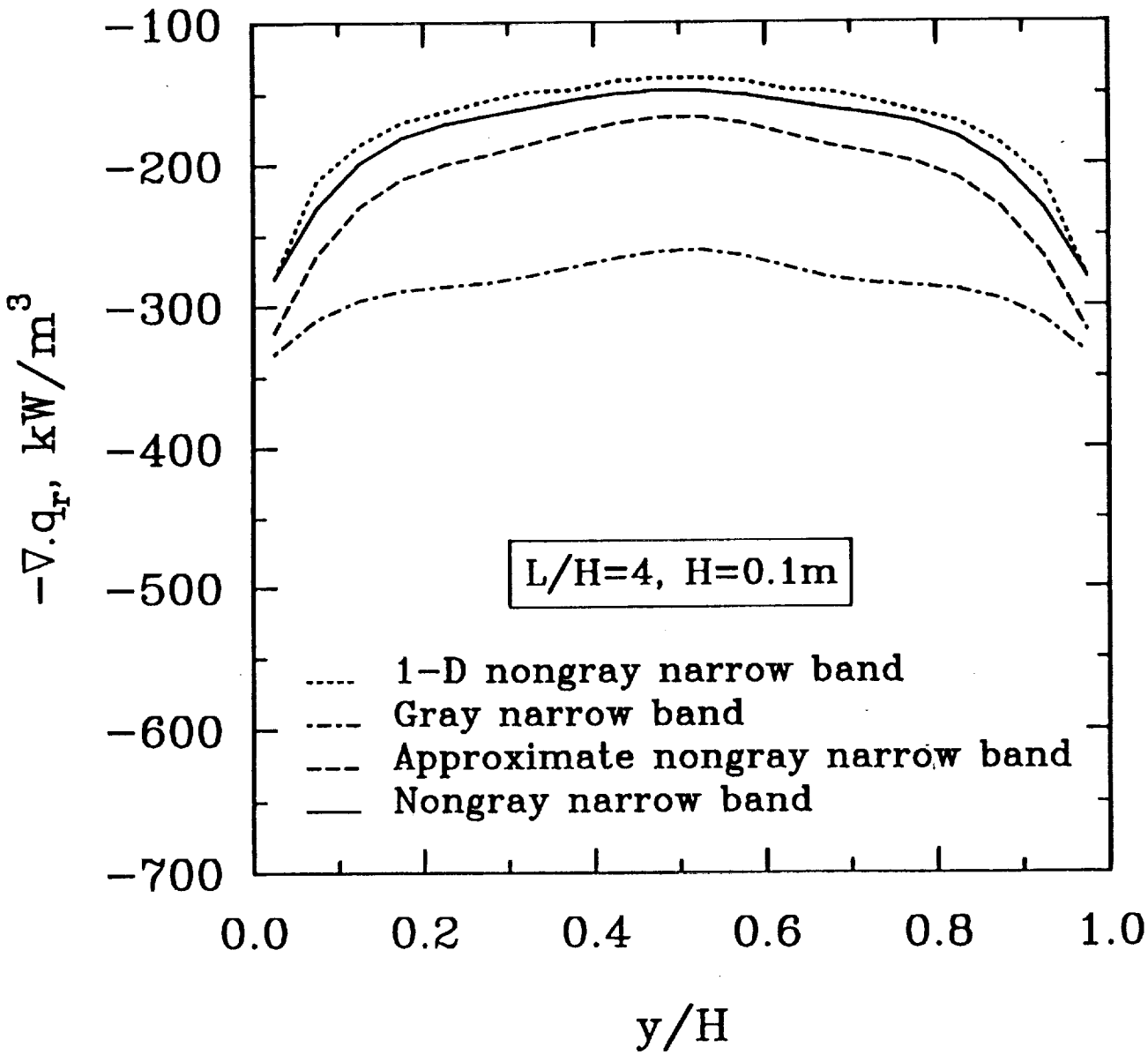

Fig. 5.3(b) Radiative dissipation at middle location for the case of uniform temperature (L/H=4).

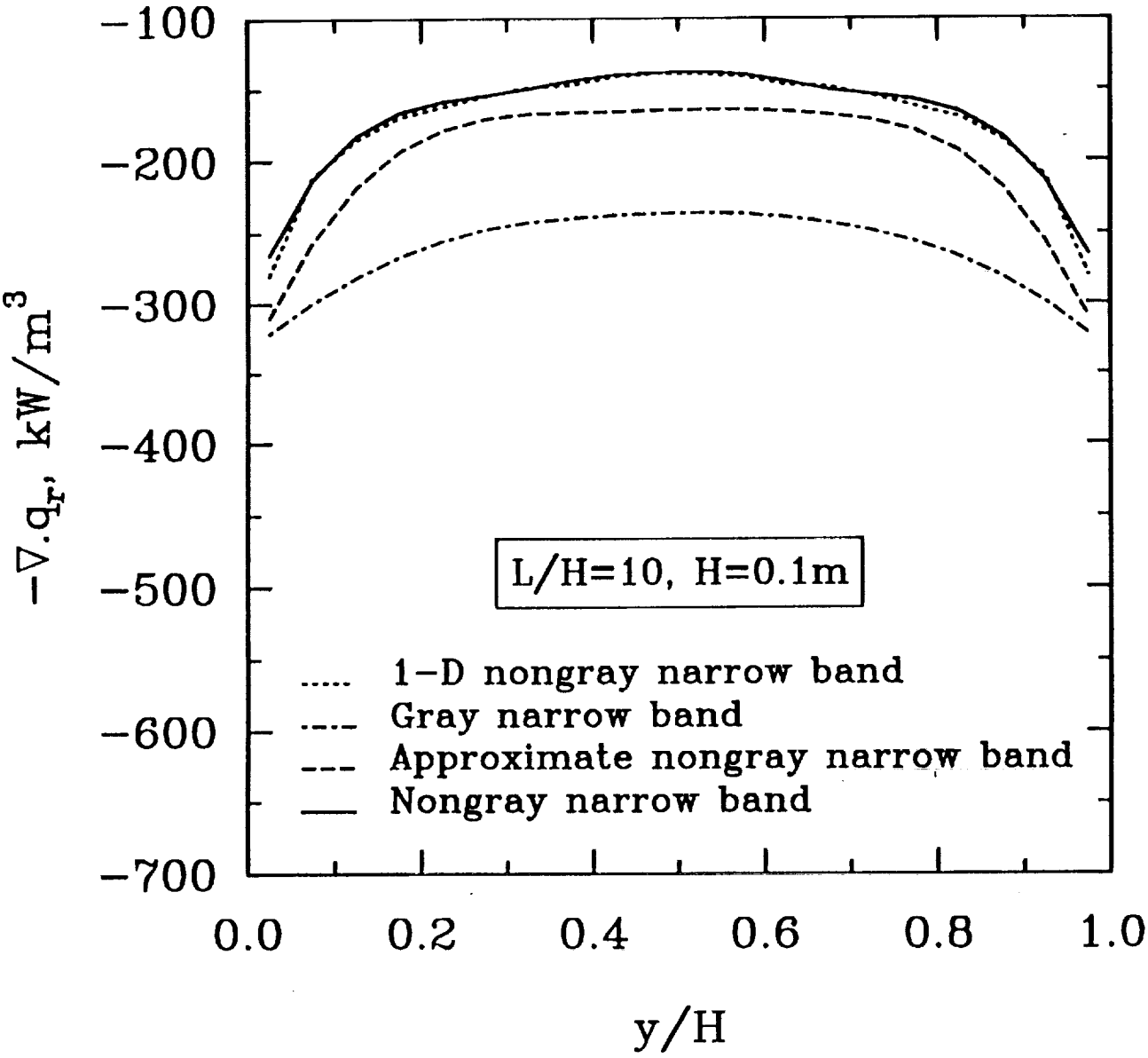

Fig. 5.3(c) Radiative dissipation at middle location for the case of uniform temperature (L/H=10).

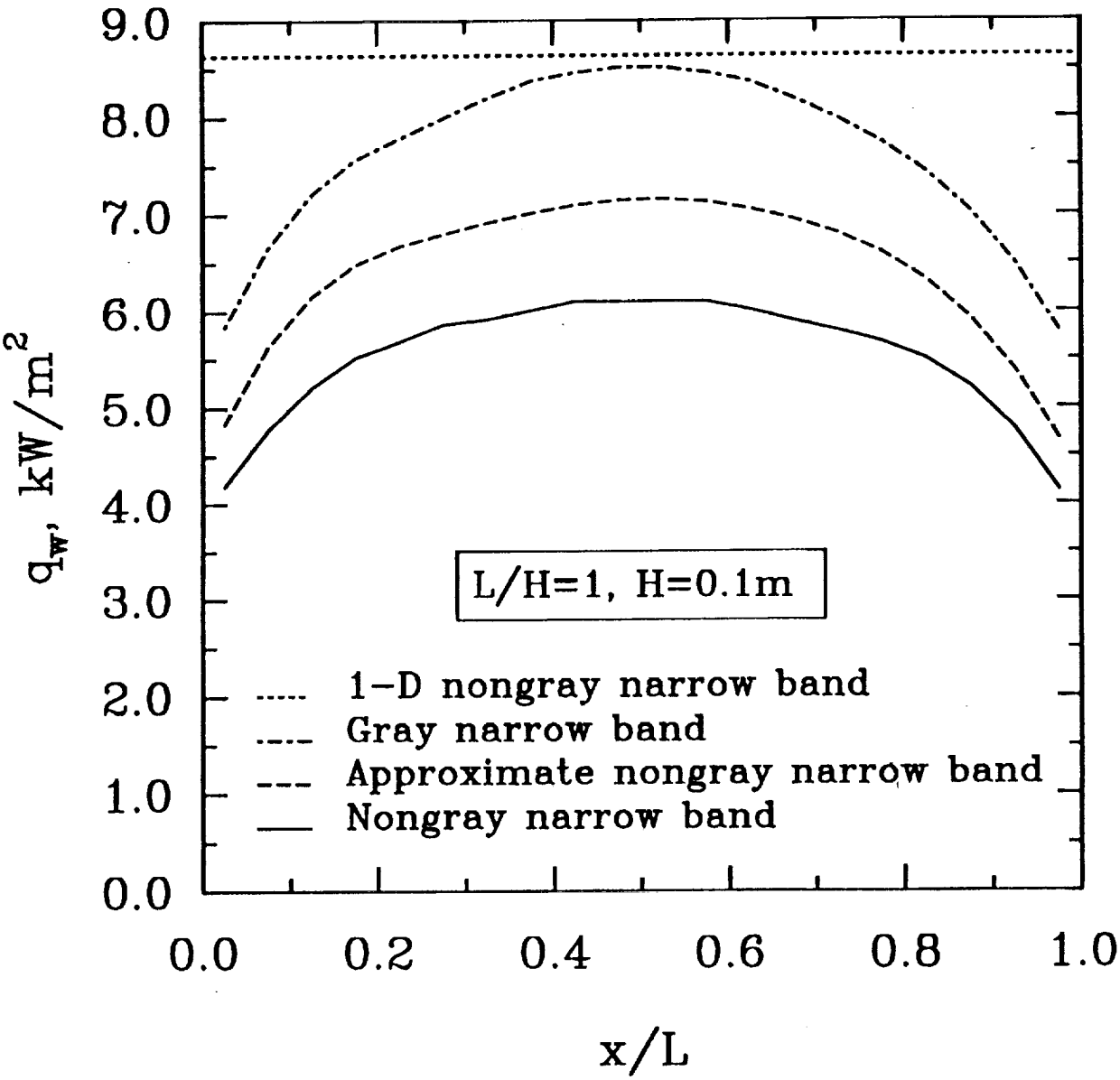

Fig. 5.3(d) Radiative wall flux distribution for the case of uniform temperature (L/H=1).

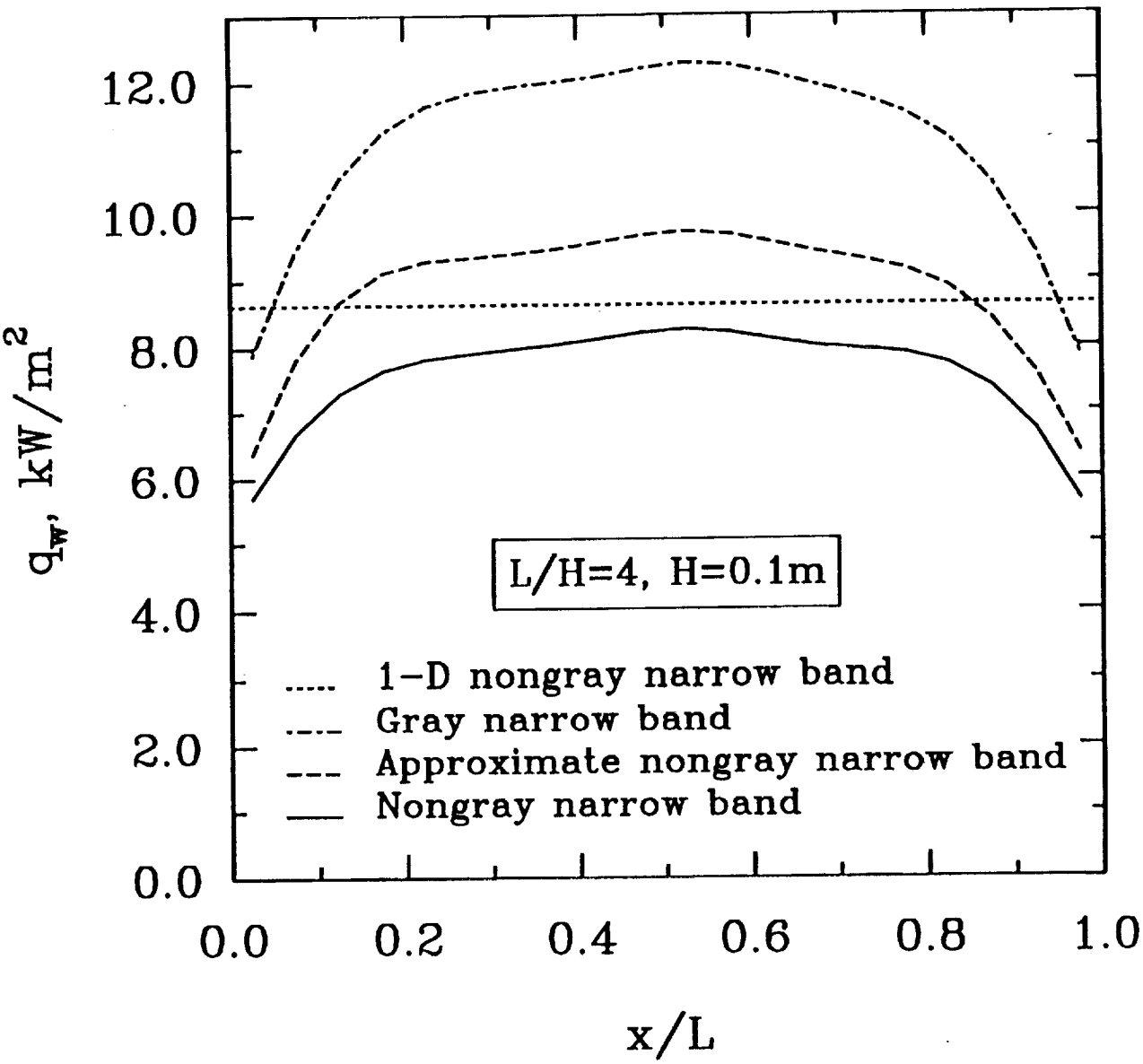

Fig. 5.3(e) Radiative wall flux distribution for the case of uniform temperature (L/H=4).

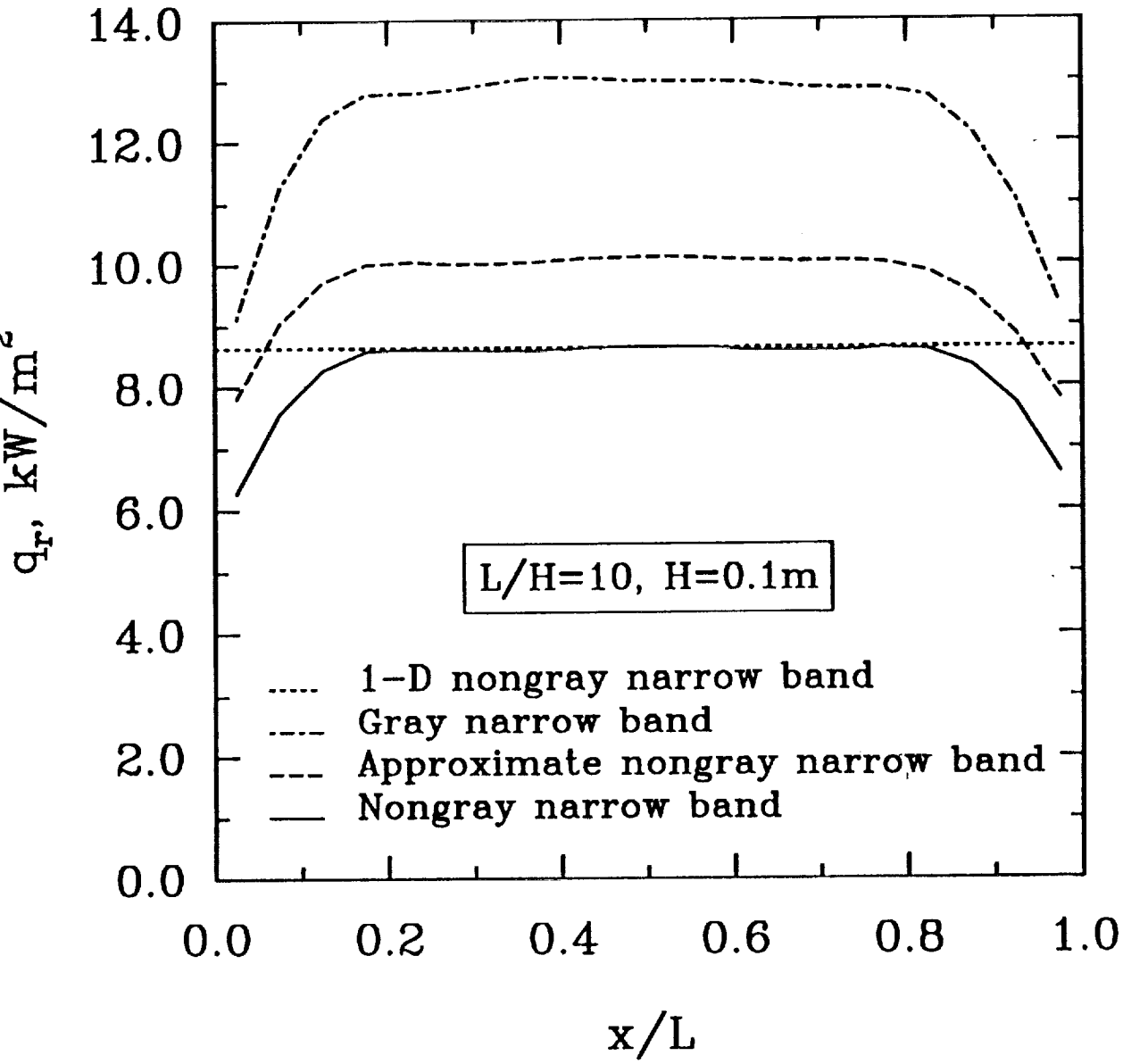

Fig. 5.3(f) Radiative wall flux distribution for the case of uniform temperature (L/H=10).

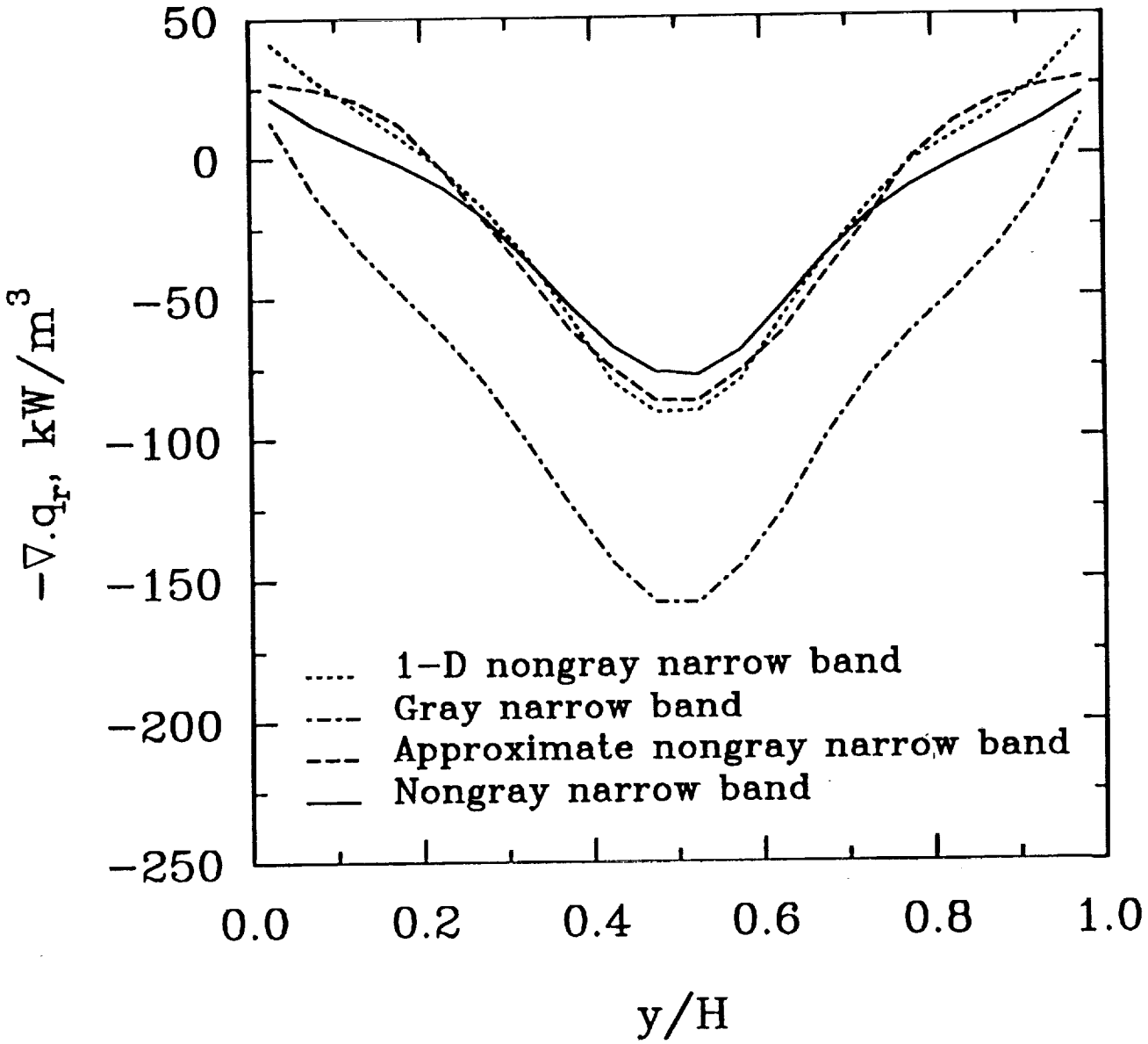

Fig. 5.4(a) Radiative dissipation at the location(x/L =0.275) for the case of nonuniform temperature.

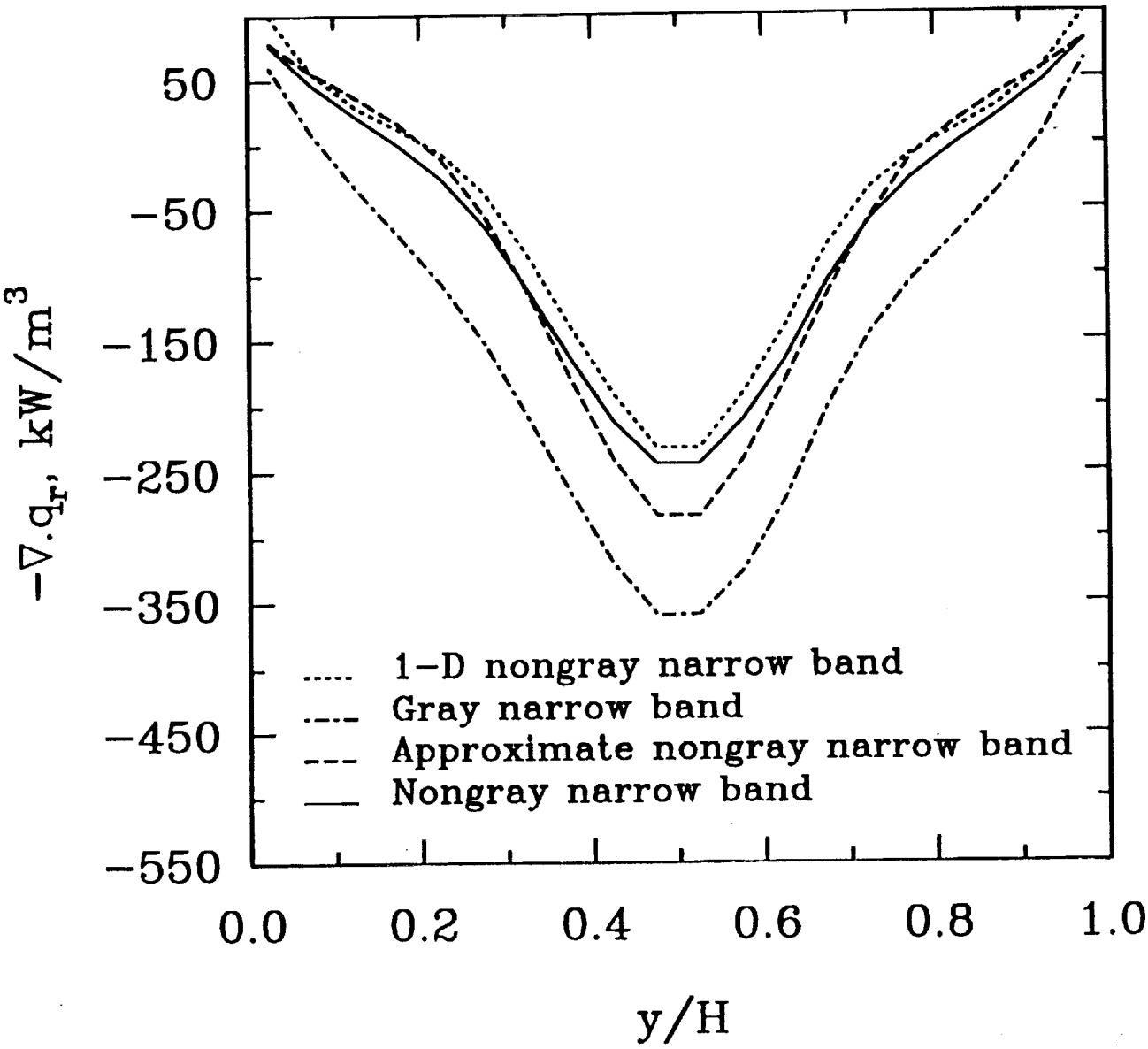

Fig. 5.4(b) Radiative dissipation at the location(x/L =0.575) for the case of nonuniform temperature.

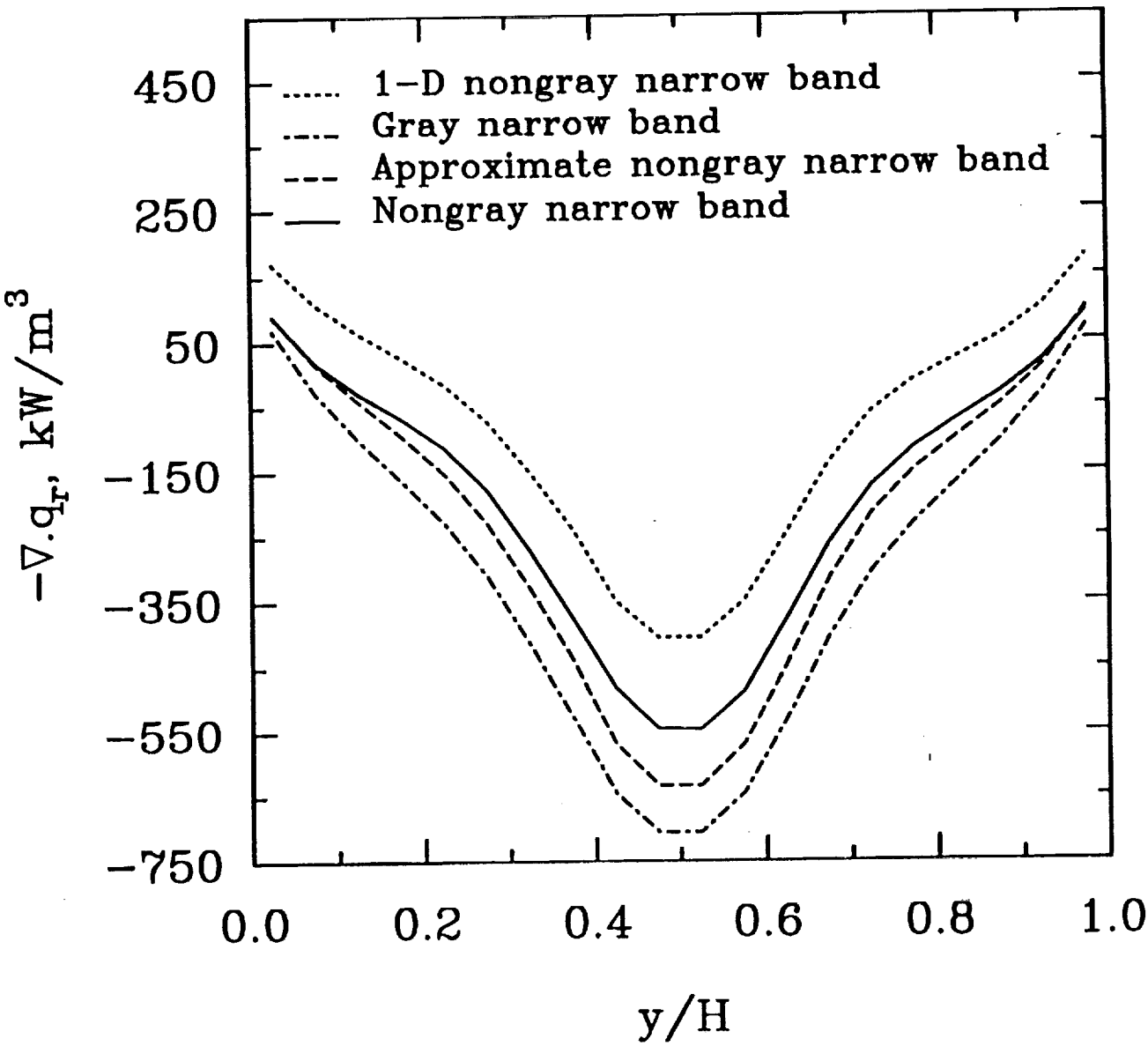

Fig. 5.4(c) Radiative dissipation at the location(x/L =0.875) for the case of nonuniform temperature.

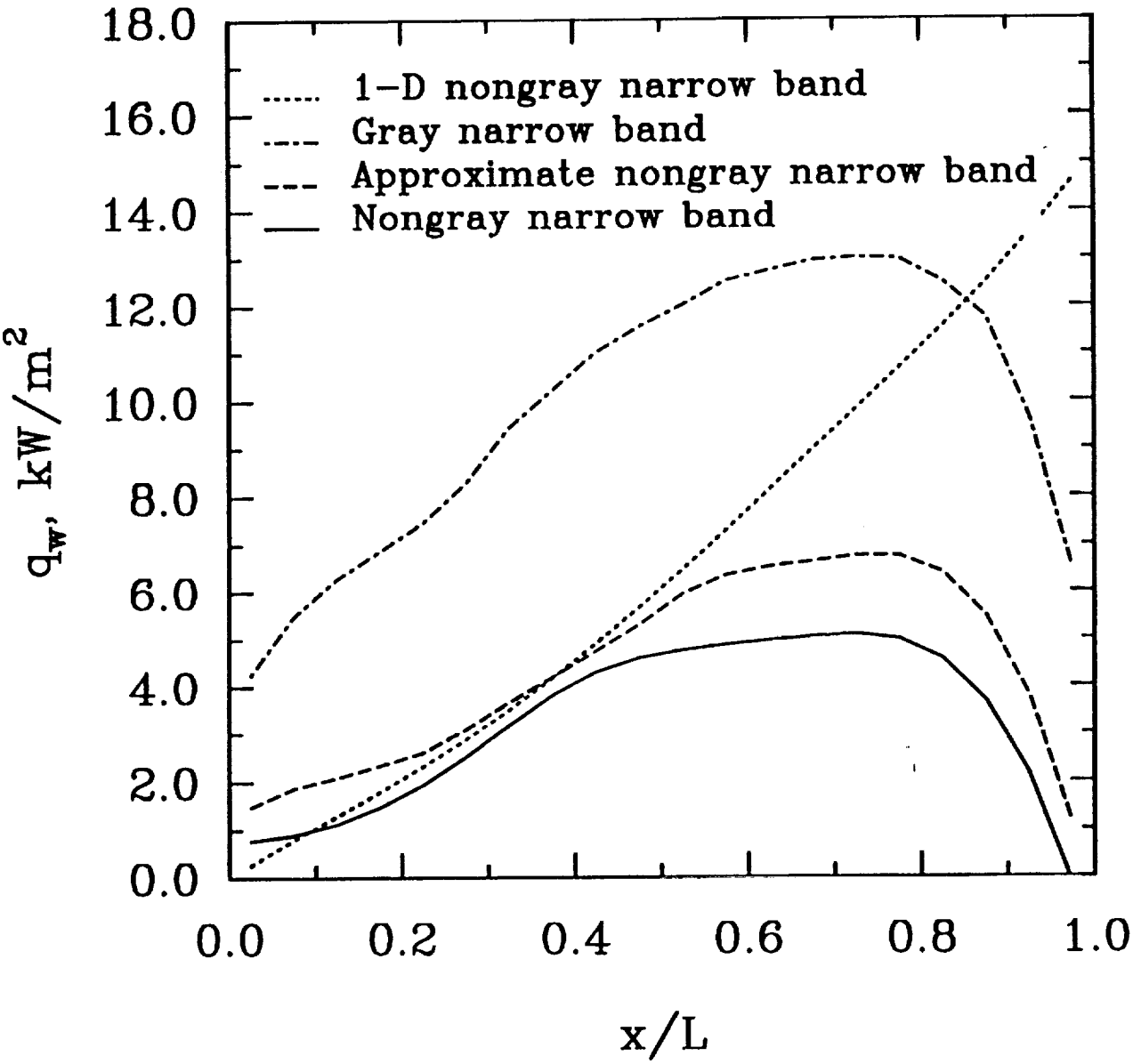

Fig. 5.4(d) Radiative wall flux distribution for the case of nonuniform temperature.

6. CONCLUDING REMARKS

A brief review is represented on various radiation absorption models. One of the most accurate narrow band model is chosen to investigate the radiative heat transfer using the MCM. The spectral correlation between transmittances of two different segments of the same path in a medium makes statistical relationship different from the conventional relationship that only provides the noncorrelated results for nongray analysis. For the nongray case with reflecting walls, the advantages of the MCM are very clear in comparison to other methods.

Extension of a one-dimensional problem to a multi-dimensional problem requires some special treatments in the Monte Carlo analysis. The Monte Carlo statistical relationships should be derived from the independent terms in the formulation of total emitted radiative energy within a volume element. Use of different assumptions results in different sets of Monte Carlo formulations. Comparisons among the nongray, approximate nongray and gray solutions as well as one-dimensional nongray solution for the cases with uniform and nonunifrom temperature distributions have demonstrated that one-dimensional treatment cannot simulate the radiative heat transfer correctly in the region where two-dimensional effects are dominant. The gray solution usually differs from the nongray solution significantly. The differences between the approximate nongray solution and the nongray solution are lower than those between the gray and the nongray solutions. In some cases the approximate nongray solution may not be acceptable.

Edwards, D. K., 1983, "Numerical Methods in Radiation Heat Transfer," in: Numerical Properties and Methodologies in Heat Transfer, T. M. Shih, ed., Hemisphere, Washington, D. C., 1983, pp. 479–496.

Edwards, D. K. and Babikian, P. S., 1989, "Radiation from a Nongray Scattering, Emitting and Absorbing SRM Plume," AIAA Paper No. 89–1721.

Farmer, J. F., and Howell, J. R., 1992, "Monte Carlo Solution of Radiative Heat Transfer in a Three-dimensional Enclosure with an Anisotropically Scattering, Spectrally Dependent, Inhomogeneous Medium," Proceedings of the 28th National Heat Transfer Conference, San Diego, California, ASME HTD-Vol. 203, August 1992, pp. 301–309.

Godson, W. L., 1953, "The Evaluation of Infrared Radiation Fluxes Due to Atmospheric Water Vapor," Quarterly Journal of Royal Meteorological Society, Vol. 79, pp. 367–379.

Goody, R. M., 1964, Atmospheric Radiation, Oxford Press, London, pp. 234–243, 1964.

Gupta, R. P., Wall, T. F., and Truelove, J. S., 1983, "Radiative Scatter by Fly Ash in Pulverized-Coal-Fired Furnaces: Application of the Monte Carlo Method to Anisotropic Scatter," International Journal of Heat and Mass Transfer, Vol. 26, No. 11, November 1983, pp. 1649–1660.

Haji-Sheikh, A., 1988, "Monte Carlo Methods," in: Handbook of Numerical Heat Transfer, W. J. Minkowycz, E. M. Sparrow, G. E. Schneider and R. H. Pletcher, eds., Wiley, New York, Chapter 16.

Hartmann, J. M., Levi Di Leon, R., and Taine, J., 1984, "Line-by-line and Narrow-band Statistical Model Calculations for H_2O," Journal of Quantitative Spectroscopy and Radiative Transfer, Vol. 32, No. 2, February 1984, pp. 119–127.

Howell, J. R., 1968, "Application of Monte Carlo to Heat Transfer Problems," Advances in Heat Transfer, Vol. 5, Academic Press, New York.

Howell, J. R., 1983, "Radiative Transfer in Multidimensional Enclosures with Participating

Media," ASME Paper 83–HT-32, 1983.

Howell, J. R, 1988, "Thermal Radiation in Participating Media: The Past, the Present, and Some Possible Futures," Journal of Heat Transfer, Vol. 110, November 1988, pp. 1220–1229.

Howell, J. R., and Perlmutter, M., 1964a, "Monte Carlo Solution of Thermal Transfer through Radiant Media between Gray Walls," Journal of Heat Transfer, Vol. 86, February 1964, pp. 116–122.

Howell, J. R., and Perlmutter, M., 1964b, "Monte Carlo Solution of Radiant Heat Transfer in a Nongray Nonisothermal Gas with Temperature Dependent Properties," American Institute of Chemical Engineers Journal, Vol. 10, No. 4, July 1964, pp. 562–567.

Kim, T. K., Menart, J. A., and Lee, H. S., 1991a, "Nongray Radiative Gas Analyses Using the S-N Discrete Ordinates Method," Journal of Heat Transfer, Vol. 113, November 1991, pp. 946–952.

Kim, T. K., Menart, J. A., and Lee, H. S., 1991b, "S-N Discrete Ordinates Solutions of Nongray Radiative Transfer with Diffusely Reflecting Walls," Proceedings of the 28th National Heat Transfer Conference, Minneapolis, Minnesota, ASME HTD-Vol. 160, July 1991, pp. 79–87.

Kobiyama, M., Taniguchi, H. ,and Saito, T., 1979, "The Numerical Analysis of Heat Transfer Combined with Radiation and Convection," Bulletin of the Japan Society of Mechanical Engineers, Vol. 22, No. 167, May 1979, pp. 707–714.

Kobiyama, M., 1986, "A Study on the Reduction of Computing Time of the Monte Carlo Method Applied to the Radiative Heat Transfer," Bulletin of the Japan Society of Mechanical Engineers, Vol. 29, No. 255, September 1986, pp. 3000–3006.

Kumar, A., 1986, "Numerical Simulation of Scramjet Inlet Flowfield," NASA TP-25117, May 1986.

Ludwig, C. B., Malkmus, W., Reardon, J. E., and Thompson, J. A. L., 1973, "Handbook of

Infrared Radiation from Combustion Gases," NASA SP-3080.

Malkmus, W., 1967, "Random Lorentz Band Model with Exponential-tailed S^{-1} Line-intensity Distribution Function," Journal of the Optical Society of America, Vol., No. 3, pp. 323–329.

Menart, J. A., Lee, H. S., and Kim, T. K., 1993, "Discrete Ordinates Solutions of Nongray Radiative Transfer with Diffusely Reflecting Walls," Journal of Heat Transfer, Vol. 115, February 1993, pp. 184–193.

Modest, 1992, "The Monte Carlo Method Applied to Gases with Spectral Line Structure," Proceedings of the 28th National Heat Transfer Conference, San Diego, California, ASME HTD-Vol. 203, August 1992, pp. 79–84.

Perlmutter, M. and Howell, J. R., 1964, "Radiative Transfer through a Gray Gas between Concentric Cylinders Using Monte Carlo," Journal of Heat Transfer, Vol. 86, May 1964, pp. 169–179.

Siegel, R., and Howell, J. R., 1981, Thermal Radiation Heat Transfer, McGraw-Hill Book Co., New York, 1971; Second Edition, 1981.

Soufiani, A., Hartmann, J. M., and Taine, J., 1985, "Validity of Band-model Calculation for CO_2 and H_2O Applied to Radiative Properties and Conductive-radiative Transfer," Journal of Quantitative Spectroscopy and Radiative Transfer, Vol. 33, No. 3, March 1985, pp. 243–257.

Soufiani, A., and Taine, J., 1987, "Application of Statistical Narrow-band Model to Coupled Radiation and Convection at High Temperature," International Journal of Heat and Mass Transfer, Vol. 30, No. 3, March 1987, pp. 437–447.

Sparrow, E. M., and Cess, R. D., 1978, Radiation Heat Transfer, Augmented Edition, Hemisphere Publishing Corporation, Washington, D. C..

Steward, F. R., and Cannon, P., 1971, "The Calculation of Radiative Heat Flux in a Cylindrical Furnace Using the Monte Carlo Method," International Journal of Heat and Mass

Transfer, Vol. 14, No. 2, February 1971 , pp. 245–262.

Taniguchi, H., Kudo, K., Otaka, M., Sumarsono, M., and Obata, M., 1991, "Non-gray Analysis on Radiative Energy Transfer through Real Gas Layer by Monte Carlo Method," Proceedings of the 7th International Conference on Numerical Methods of Thermal Problems.

Tiwari, S. N., 1978, "Models for Infrared Atmospheric Radiation," Advances in Geophysics, Vol. 20, Academic Press, New York, 1978.

Thynell, S., 1989, "Effect of Either CO_2 and H_2O and Particles on Radiation in a One-dimensional Cylinder," AIAA Paper No. 89–1718.

Zhang, L., Soufiani, A., and Taine, J., 1988, "Spectral Correlated and Non-correlated Radiative Transfer in a Finite Axisymmetric System Containing an Absorbing and Emitting Real Gas-particle Mixture," International Journal of Heat and Mass Transfer, Vol. 31, No. 11, November 1988, pp. 2261–2272.